Sedimentology (2008) **55,** 729–750 doi: 10.1111/j.1365-3091.2007.00919.x

Dolomite–silica stromatolites in Miocene lacustrine deposits from the Duero Basin, Spain: the role of organotemplates in the precipitation of dolomite

MARÍA E. SANZ-MONTERO*†, JUAN P. RODRÍGUEZ-ARANDA*† and MARÍA A. GARCÍA DEL CURA†‡
**Dpto. Petrología y Geoquímica, Facultad de Geología, Universidad Complutense de Madrid, C/ Antonio Novais, 2, 28040 Madrid, Spain (E-mail: mesanz@geo.ucm.es)*
†Instituto de Geología Económica, CSIC-UCM, Facultad de Geología, Madrid, Spain
‡Laboratorio de Petrología Aplicada, Unidad Asociada CSIC-UA, Alicante, Spain

Associate Editor: John Reijmer

ABSTRACT

This research provides an ancient analogue for biologically mediated dolomite precipitation in microbial mats and biofilms, and describes the involvement of highly structured extracellular polymeric secretion (EPS) templates in dolomite nucleation. The structure of EPS is shown to match the hexagonal–trigonal lattice geometry of dolomite, which favoured the epitaxial crystallization of dolomite on the organic substrate. This structure of EPS also matches the arrangement of silica nanospheres in opal, which further accounts for the organically-templated formation of opal enabling the non-replacive co-existence of dolomite and silica. The study is focused on a 50 m thick dolomite succession that is exposed in central areas of the Tertiary Duero Basin and was deposited in a mudflat-saline lake sedimentary complex during the Middle to Late Miocene (9 to 15 Ma). In the intermediate intervals of the succession, poorly indurated dolomite beds pass gradually into silica beds. On the basis of sedimentological, compositional, geochemical and petrographic data, silica and dolomite beds have been interpreted as mineralized microbial mats. The silica beds formed in marginal areas of the lake in response to intense evaporative concentrations; this resulted in the rapid and early precipitation of opal. Silicification accounted for the exceptional preservation of the microbial mat structure, including biofilms, filamentous and coccoid microbes, and EPS. Extracellular polymeric secretions have a layered structure, each layer being composed of fibres which are arranged in accordance with a reticular pattern, with frequent intersection angles at 120° and 60°. Therefore, the structure of EPS matches the lattice geometry of dolomite and the arrangement of silica nanospheres in opal. Additionally, EPS binds different elements, with preference to Si and Mg. The concurrence of suitable composition and surface lattice morphologies in the EPS favoured the crystallization of dolomite on the substrate. In some cases, dolomite nucleation took place epicellularly on coccoid micro-organisms, which gave way to spheroid crystals. Organic surfaces enable the inorganic mineral precipitation by lowering the free energy barrier to nucleation. Most of the microbial mats probably developed on the lake floor, under sub-aqueous conditions, where the decomposition of organic matter took place. The subsequent formation of openly packed dolomite crystals, with inter-related Si-enriched fibrils throughout, is evidence for the pre-existence of fibrillar structures in the mats. Miocene dolomite crystals are poorly ordered and non-stoichiometric,

with a slight Ca-excess (up to 5%), which is indicative of the low diagenetic potential the microbial dolomite has towards a more ordered and stoichiometric structure; this confirms that microbial imprints can be preserved in the geological record, and validates their use as biosignatures.

Keywords Dolomite, Duero Basin, lake, microbialite, Miocene, organic-templated nucleation, silica.

INTRODUCTION

In spite of the geochemical problems involved in the precipitation of dolomite under earth surface conditions, this process in fact takes place in some saline environments under the necessary hydro-geochemical conditions (Last, 1990). In order to explain this phenomenon, Vasconcelos & McKenzie (1997) and Wright (1999) attributed this to microbial participation. According to these authors, in saline, magnesium-rich waters the nucleation of dolomite is due to metabolic microbial reactions which can change the composition of solutions to such an extent that kinetic inhibitors can be overcome. The recognition of biologically mediated dolomite in recent lacustrine sediments in the Gallocanta wetland (north-east of Spain) expands the range of environmental conditions conducive to dolomite precipitation from coastal areas to inland saline lakes (Corzo *et al.*, 2005).

Direct observations in coastal areas of Brazil (Vasconcelos *et al.*, 1995), and Australia (Wright, 1999) and in an inland lake in Spain (Corzo *et al.*, 2005) have demonstrated that sulphate-reducing bacteria influence dolomite precipitation under low-temperature, anoxic conditions. The bacterial sulphate reduction processes may overcome the kinetic barrier to dolomite formation by increasing pH and carbonate alkalinity (Warthmann *et al.*, 2000).

Similarly, studies conducted on microbial mats, the modern analogues of stromatolites, also highlighted that the sulphate reduction processes are not only responsible for the formation of carbonate laminae but are also implicated in the lithification of modern stromatolites both in marine environments (Reid *et al.*, 2000; Visscher *et al.*, 2000) and in moderate hypersaline settings (Warthmann *et al.*, 2005).

It is generally assumed that early-formed dolomites undergo recrystallization during the diagenesis (Tucker & Wright, 1990). This assumption may make it difficult to recognize microbial dolomite in the rock record. Vasconcelos & McKenzie (1997) found a diagenetic trend towards more ordered and stoichiometric dolomite with burial depth, and consequently with time, in the recent sediments of Lagoa Vermelha (Brazil). Wright (1999) suggests a similar pattern from the sludge dolomite sediments in the Coorong lakes in Australia. Apparently, this process would finally result in coarse, nearly stoichiometric and well-ordered crystals. The study of ancient dolomite deposits can provide some clues to deciphering pathways of dolomite transformation throughout time and would help to validate the evolutionary hypotheses (Calvo *et al.*, 2003).

Dolomite beds are widely recorded in the Neogene lake deposits from Spain. Some studies conducted in these deposits have shown that microbes also played a role in the formation of ancient dolomites (García del Cura *et al.*, 2001; Calvo *et al.*, 2004; Sanz-Montero *et al.*, 2006a,c). In addition, the paper by Sanz-Montero *et al.* (2006c) provides a model for the early replacement of gypsum by microbial dolomite, which indicates the importance of gypsum precipitates as a source of SO_4^{2-} in order to fuel the sulphate-reducing bacteria in the process of dolomite formation. This model differs from the geological sites in which primary dolomite is precipitating at the present time where SO_4^{2-} ions are considered to be supplied to the water bodies in a solution from external sources.

Silicification of carbonates is a common diagenetic process observed in ancient lacustrine facies (Bustillo *et al.*, 2002). The precise mechanisms operating in carbonate replacement by silica are often controversial (Hesse, 1990), and are, therefore, not yet fully explained; this shows the need to study dolomite and interbedded deposits in order to shed light on the formation and further diagenesis of microbial dolomite.

The aim of this paper was to analyse the microbial involvement in the formation and subsequent diagenetic evolution of Miocene dolomite facies deposited in a mudflat-saline lake system of the Duero Basin. Dolomite occurs intimately interdigitated with silica beds, which

resulted from the silicification of microbial mats. The silicification processes operated early and this accounts for the exceptional preservation of the microbial ultrastructure. The results from the detailed study of these structures give new insight into the non-replacive relationships between silica and dolomite. In addition, the results enhance the role of the organic templates in the precipitation of dolomite and silica. The organic templates provide the minerals with a suitable formation micro-environment, including a paracrystalline structure that may act as nucleation site, and as a reservoir to supply Mg and Si.

GEOLOGICAL SETTING

The study area is located in the vicinity of the village of Cuéllar (Segovia province, Spain) which lies in the centre of the continental Tertiary Duero Basin (Fig. 1). The Duero Basin is an intraplate endorheic depression located in the north-western region of the Iberian Peninsula. The up to 3000 m thick sedimentary record in the basin spans from Late Cretaceous–Early Palaeocene to Late Miocene–Pleistocene (Alonso-Gavilán *et al.*, 2004). According to Armenteros *et al.* (2002), seven main sedimentary stages, or lithostratigraphic units, have been distinguished and these are controlled by the tectonic activity in the basin margins, as well as in the basin floor.

The study materials deposited during the sedimentary 'stage 5' (Middle–Late Miocene) are included in the Intermediate Unit of the Miocene (García del Cura, 1974) which is referred to as the 'Cuestas Unit' (Alonso-Gavilán *et al.*, 2004) towards the centre of the basin. The 'Cuestas Unit' consists of limestones, dolostones, marls and gypsum (interstitial, sedimentary precipitated and detrital). Accordingly, the interpretation of the facies associations is related to dry-saline mudflat-ephemeral saline lake systems, alternating in time and space with shallow fresh water carbonate lakes (Mediavilla *et al.*, 1996; Armenteros *et al.*, 2002). The lake deposits interfinger with terrigenous deposits towards the basin margins in accordance with a typical alluvial-saline lake concentric pattern characteristic of a hydrologically closed basin. The transition area between the siliciclastic alluvial facies and the central gypsiferous lake deposits is well-defined and easily recognizable through its

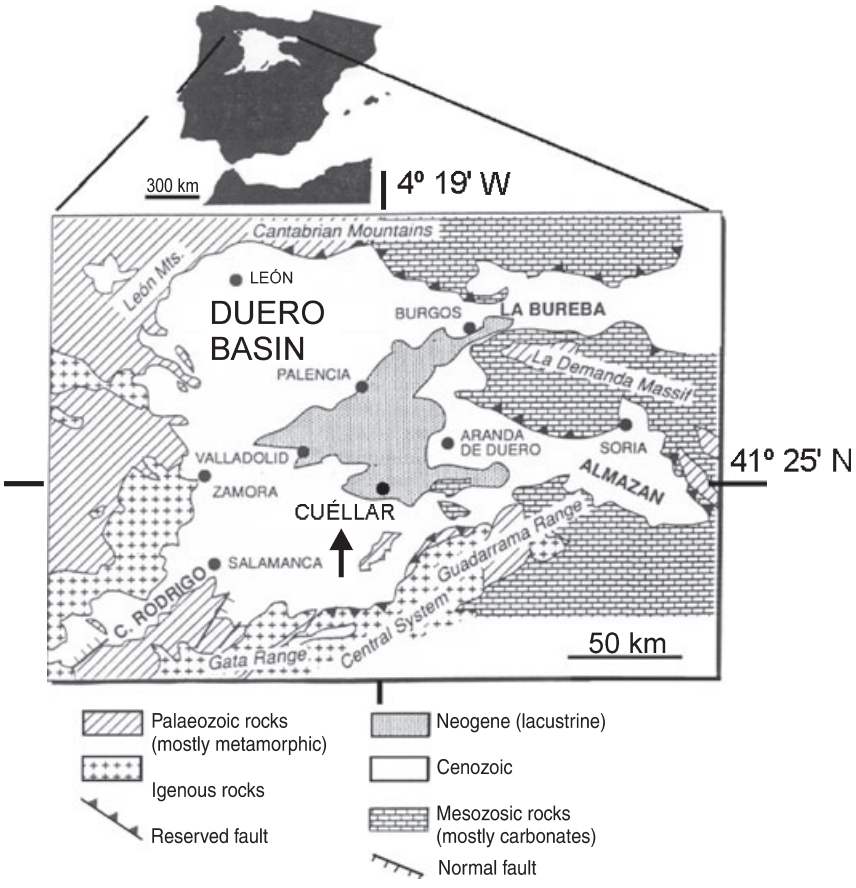

Fig. 1. Geological map of the Duero Basin, in the Northern Meseta of Spain, showing the position of the study area, village of Cuéllar (arrowed). Modified from Mediavilla *et al.* (1996).

dolomite lithology (Ordóñez *et al.*, 1981). The sedimentary 'stage 5' ends with a widespread hardened limestone horizon known as 'Lower Moor', which provides a distinctive layer for stratigraphical correlations (García del Cura, 1974; Armenteros *et al.*, 2002).

Diagenetic evolution of the studied successions has led to a maximum depth of burial of over 100 m and has not recorded any metamorphism or hydrotermalism event (Armenteros *et al.*, 2002; Alonso-Gavilán *et al.*, 2004). Thus, the features recognized in the analysed rocks have been interpreted in terms of sedimentary and/or surficial diagenetic processes.

STUDIED SECTIONS

Six horizontally bedded sections were measured within the same stratigraphic interval in a 100 km^2 area located near the village of Cuéllar (Fig. 1). These sections reveal negligible differences in thicknesses and facies variability, which make it possible to depict a representative stratigraphic section for the Intermediate Unit of the Miocene in the area (Fig. 2).

The stratigraphic section is 80 m thick and consists mainly of carbonates, mostly dolomite.

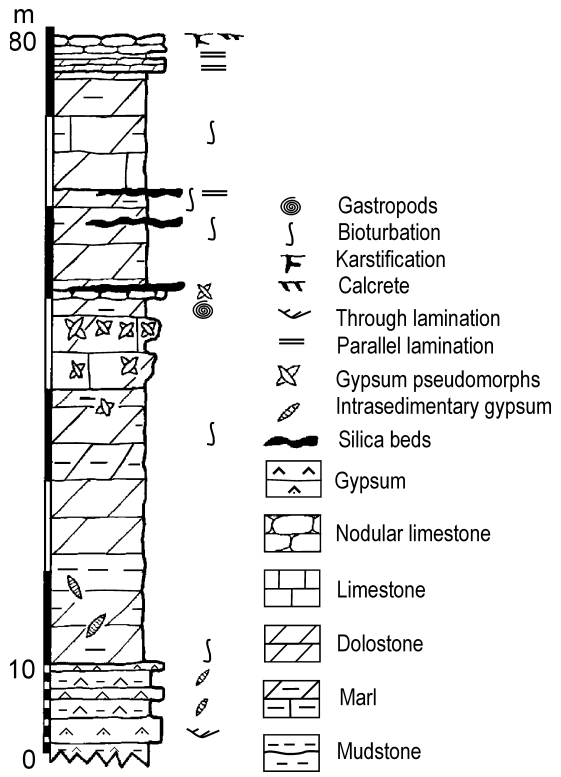

Fig. 2. Generalized sedimentary log of the dolomite succession studied near the village of Cuéllar.

The lower part of the section is composed of detrital gypsum and gypsiferous mudstones. Reworked gypsum is represented by sheet-like beds, 10 to 20 cm thick, which have erosive bases locally. The beds are composed of sand-sized gypsum grains showing through cross-bedding. These beds are interlayered with centimetre-thick greenish to reddish mudstones which contain abundant intra-sedimentary gypsum crystals. The present study is focused on the middle part of the section, up to 55 m thick, which comprises a succession of poorly indurated, bioturbated, white to cream, massive dolomite beds (Figs 2 and 3). The basal part of the dolomite succession is 30 m thick, and includes thin deposits of dolomarlstone and lenticular gypsum crystals or moulds. In the overlying 10 m thick interval, dolomite facies are interbedded with carbonate pseudomorphs after gypsum aggregates that are associated with porous limestone beds. The topmost porous limestone layer can be recognized over an area of 30 km^2. Above this, a 12 m thick interval of the succession contains up to a maximum of 4 dm thick silica beds, laterally continuous for tens of metres. Locally, dolomites occur interlayered with centimetre-thick clayey dolomarlstone beds. A hardened crust made of diagenetic limestones (Mediavilla & Dabrio, 1989), referred to as 'Lower Moor', represents the upper limit of the Intermediate Unit of the Miocene in the area (Fig. 2).

MATERIALS AND METHODS

Standard petrographic analyses of 50 samples were used to describe the dolomite–silica stromatolites and associated facies (limestone, gypsum and mudstone). Additionally, UV-fluorescence microscopy images of thin sections were obtained with an Olympus BX51 (Olympus, Tokyo, Japan), equipped with an U-RFL-T power supply unit, to evaluate the presence and distribution of light hydrocarbons and organic matter in the samples.

For high-resolution textural analysis of silica and dolomite rocks, fresh broken surfaces of previously air-dried samples were studied with scanning electron microscopy provided with X-ray energy-dispersive spectroscopy (SEM-EDS) [JEOL JSM-840 (JEOL, Tokyo, Japan) and Hitachi S-3000N (Hitachi Ltd, Tokyo, Japan)], and with field emission scanning electron microscopy (FE-SEM) (JEOL JM-6400). To obtain more precise elemental analyses, uncoated polished surfaces

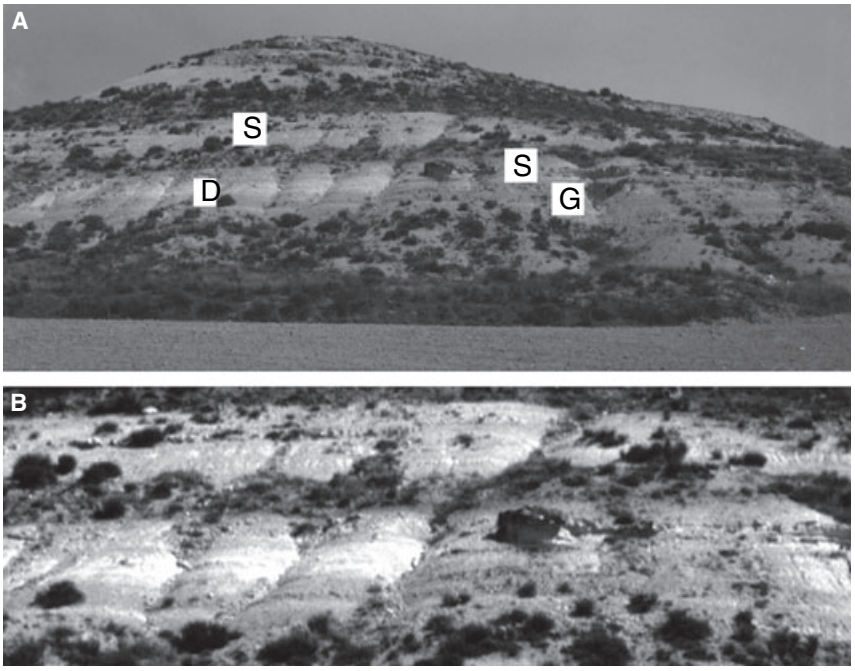

Fig. 3. Outcrop of the dolomite succession in the vicinity of Cuéllar. (A) General view. White dolomite facies (D) pass gradually into indurated silica beds (S) and/or calcite pseudomorphs after gypsum (G). Outcrop thickness is 50 m. (B) Magnified view showing the facies transitions.

were studied with the Hitachi S-3000 N equipment, which was operated in a low vacuum.

Electron-microprobe (EMP) quantitative spot analyses and elemental mappings of the samples were carried out in wavelength-dispersive mode, using a JEOL Superprobe JXA 8900-M (JEOL) equipped with four crystal spectrometers. Operating conditions were as follows: acceleration voltage of 20 kV and probe current of 50 nA, with variable counting times between 10 and 30 sec and between 5 and 15 sec, in peak and background, respectively. Beam diameter was between 2 and 5 μm in order to minimize damage from the electron beam. Backscattered electron imaging was used in order to examine the compositional heterogeneities of the samples.

X-ray diffraction of the whole rock was used to determine mineral composition in powdered samples, using quartz as an internal standard. The equipment used was a Philips X-ray diffraction system (Royal Philips Electronics, Amsterdam, The Netherlands) operated at 40 kV and 30 mA, and monochromated Cu-K_α radiation. Semi-quantitative estimates of relative percentages of minerals from whole-rock samples were made through measurement of intensity of the diffraction peaks by integration of the area. Values of mol.% $CaCO_3$ of the carbonate minerals were estimated by measurement of the position of the d_{104} peak relative to a standard (Goldsmith *et al.*, 1961). The degree of ordering of the dolomite crystals was determined by the sharpness and relative intensities of the ordering peaks, superstructure reflections corresponding to d_{021}, d_{015} and d_{110} (Goldsmith & Graf, 1958). The degree of ordering is thus estimated by the ratio of the heights of the ordering peak 015 to diffraction peak 110 (Hardy & Tucker, 1988). Orientated samples were also examined by X-ray diffraction for the determination of clay minerals in mudrocks.

Stable carbon and oxygen isotopes were used for further analyses of the origin of dolomite. Seventeen selected samples were ground down in order to pass through a 100-mesh sieve; the 250-mesh fraction was saved for analysis. Carbon dioxide was evolved from each sample at 25 °C using 100% H_3PO_4. The gas evolved in the first hour was attributed to calcite; the gas evolved between 24 hours and seven days was attributed to dolomite. All samples were prepared and analysed, at least in duplicate. The analytical precision is generally +/−0·10‰ for carbon and +/−0·15‰ for oxygen. Both oxygen and carbon values are reported in permil relative to the standard PDB (for Pee Dee Belemnite) (Table 1).

FACIES ANALYSIS

For descriptive purposes, four main facies have been distinguished according to the dominant mineralogical composition of the beds, although in many cases they occur intermixed. The facies description is followed by a brief interpretation, which takes into account the general sedimentary

Table 1. Mineralogical and compositional data of the dolomite in the different facies as determined by XRD and isotopic techniques. Minimum and maximum values, average and standard deviation are specified.

	X-ray diffraction data			Isotope data		
Dolomite facies	No. of samples	Degree of ordering	% $CaCO_3$ in dolomite	No. of samples	$\delta^{13}C_{PDB}$ (‰)	$\delta^{18}O_{PDB}$ (‰)
Tabular dolomite beds (open lake)	7	(0·33)–(0·59) av. 0·49 $\sigma = 0{\cdot}08$	(53·0)–(55·5) av. 54·6 $\sigma = 0{\cdot}8$	4	(−2·67)–(−1·41) av. −2·16 $\sigma = 0{\cdot}51$	(1·27)–(2·82) av. 2·26 $\sigma = 0{\cdot}58$
Related to silica (saline mudflat)	4	(0·44)–(0·64) av. 0·58 $\sigma = 0{\cdot}08$	(49·3)–(54·0) av. 52·3 $\sigma = 1{\cdot}9$	4	(−6·24)–(−4·09) av. −4·77 $\sigma = 0{\cdot}87$	(−1·11)–(0·93) av. −0·32 $\sigma = 0{\cdot}77$
Related to gypsum pseudomorphs (saline mudflat)	8	(0·26)–(0·67) av. 0·42 $\sigma = 0{\cdot}12$	(50·3)–(53·7) av. 51·4 $\sigma = 1{\cdot}0$	9	(−6·38)–(−3·58) av. −4·83 $\sigma = 0{\cdot}82$	(−1·33)–(1·88) av. −0·30 $\sigma = 1{\cdot}09$
Dolomarlstone (pond, marsh)	2	(0·45)–(0·45) av. 0·45 $\sigma = 0{\cdot}00$	(50·0)–(50·3) av. 50·2 $\sigma = 0{\cdot}2$		–	–
Average	21	av. 0·48 $\sigma = 0{\cdot}16$	av. 52·8 $\sigma = 2{\cdot}0$	17	av. −4·17 $\sigma = 1{\cdot}38$	av. −0·60 $\sigma = 1{\cdot}30$

model of mudflat-saline lake complexes, established by Armenteros (1991).

Dolomite facies

Dolomite forms 5 to 30 cm thick tabular beds, white to cream in colour which can be superimposed in up to 20 m thick sequences (Figs 3 and 4A). Commonly, the beds are porous and friable and occasionally include lenticular gypsum crystals or moulds infilled with calcite cements. Apart from carbonate, the facies may contain up to 15% of clay minerals, mainly sepiolite and palygorskite. Detrital quartz, mica and feldspar grains are very scarce. The structure of beds ranges from massive to vaguely laminated. Locally, millimetre to centimetre-scale bioturbation traces disrupt the original bed structure (Fig. 4A).

Mainly, on the basis of petrographic, isotope and mineralogical features, described in detail in the petrography and composition section, the dolomite facies have been interpreted as stromatolites and microbialites resulting from the mineralization of laterally extensive microbial mats which covered the lake floor. Similar dolomite facies are also recognizable in correlatable sequences of the Madrid Basin (Sanz-Montero *et al.*, 2006a).

Silica facies

Silica beds are laterally continuous for many tens of metres, locally for several hundred metres, and gradually pass into dolomite beds (Fig. 3). The beds, white to grey in colour, are decimetres (10 to 50 cm) thick and are composed mainly of silica (opal CT and minor quartz) and carbonates, basically dolomite and subordinate calcite. Clay-rich laminae a few millimetres thick occur interdigitated, these contain up to 30% of sepiolite and palygorskite minerals.

Silica beds have centimetre-laminar or nodular mammilated appearances (Fig. 4B to D). In the first case, laminar beds are composed of alternating contorted layers showing massive, micronodular or millimetre-laminated textures (Fig. 4B and C). These textures can be disrupted by bioturbation up to a few millimetres in diameter (Fig. 4B). The proportions of silica and carbonate in the layers are variable. Some beds show knob-like surfaces and irregular morphologies (Fig. 4B) which resemble knobby pustular surfaces of stromatolites described by Reid *et al.* (2003).

The second type of silica bed has a nodular structure with dolomite nodules scattered throughout (Fig. 4D). The abundance of bioturbation traces in the beds indicates that the nodulation may result from bioturbation processes mainly produced by burrowing. Burrows frequently occur as unbranched cylindrical tubes averaging 0·5 cm in diameter and up to 4 cm in length, with occasional meniscated backfilling structures possibly caused by feeding and dwelling activities of invertebrates (Rodríguez-Aranda & Calvo, 1998). The nodular beds are characterized by a conchoidal fracture (Fig. 4D), whereas the laminar beds show irregular fractures.

Stratigraphically correlatable silica beds cropping out in western areas of the Duero Basin have

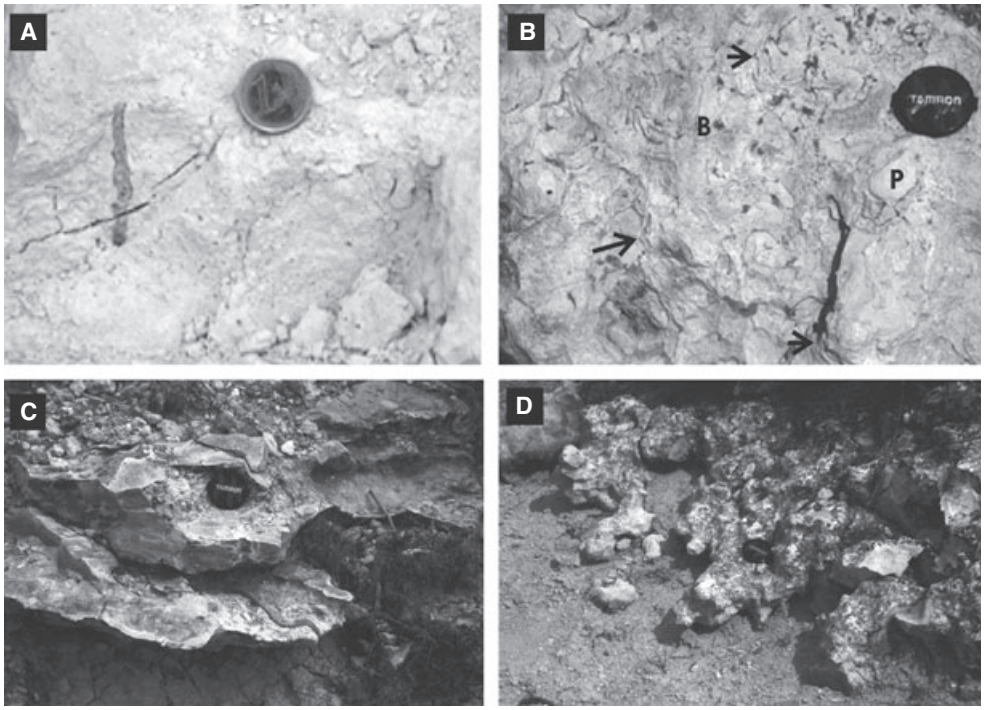

Fig. 4. Outcrop photographs. A: Poorly indurated dolomite bed showing burrowing traces. Coin for scale is 2·3 cm in diameter. B: Top surface of a laminar silica bed showing pustular morphologies (P), thin lamination (arrowed), and cylindrical burrow traces (B). C: Laminar silica beds are laminated on a cm-to-mm scale. D: Mammilated appearance of nodular silica beds. Lens cap for scale is 5 cm in diameter.

been interpreted by Armenteros *et al.* (1995) as silcretes formed by the replacement of gypsum, dolomite or mud substrates. However, a number of features, including sedimentary structures, gradual transition to dolomite facies, and microfabrics, support the interpretation that the studied silica beds may have resulted from silica precipitation in cyanobacterial mats. The abundance of burrowing and bioturbation traces is indicative of relatively diluted marginal lake conditions (Rodríguez-Aranda & Calvo, 1998). In addition, modern pustular mats are located preferentially on sites which are rarely, if ever, inundated (Stal, 1995).

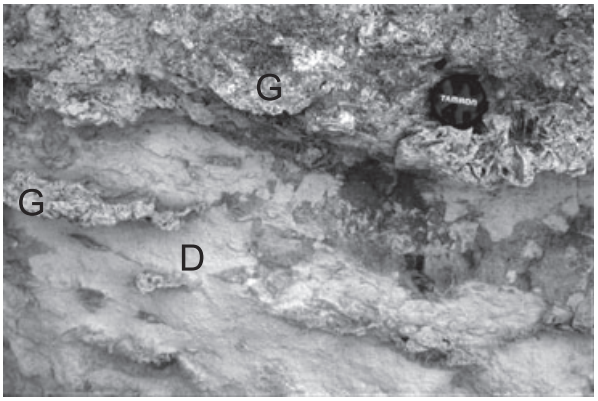

Fig. 5. Outcrop photograph of calcite pseudomorphs after rosette like gypsum aggregates (G), embedded in a dolomite bed (D). Lens cap for scale is 5 cm in diameter.

Calcite pseudomorphs after gypsum

Calcite pseudomorphs after rosette like aggregates of gypsum occur embedded in dolomite beds. The crystal size normally ranges from 1 to 30 cm and the shape is always lenticular. The rosettes occur interspersed in the dolomite groundmass or as contorted beds 10 to 50 cm thick which tend to be laterally discontinuous (Fig. 5).

The pseudomorphs consist of calcite cements which, in many cases, enclose dolomite filaments (Sanz-Montero *et al.*, 2005). According to Watson (1985), the precipitation of gypsum as aggregates took place within a sediment exposed to the vadose-to-phreatic groundwater transition zone. Subsequent gypsum dissolution could have been caused by microbial sulphate-reduction processes as suggested by Sanz-Montero *et al.* (2005).

Clayey dolomarlstone facies

Brownish thin laminated dolomarlstone is interlayered with silica and dolomite (Fig. 6). This facies is 5 to 15 cm thick and is composed of

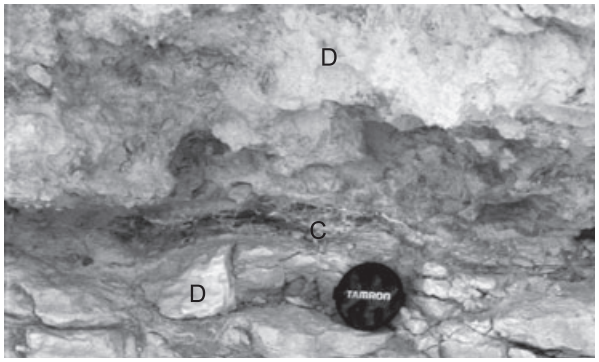

Fig. 6. Outcrop photograph of thin laminated clayey dolomarlstone (C) interlayered with dolomite (D). Lens cap for scale is 5 cm in diameter.

carbonate (dolomite and subordinate calcite), with up to 70% of clays (sepiolite, palygorskite and minor illite). Small quantities of detrital silt-sized quartz, K-feldspar and mica clasts are also present in the facies.

In the sedimentary contexts of evaporite lakes, sepiolite and palygorskite clays may be interpreted as authigenic clay deposits formed by silica-bearing waters, which were mixed with brackish or saline waters (Calvo *et al.*, 1999). Whereas, on the basis of petrographic and compositional features, dolomite associated with clays has been interpreted as having formed microbially in relation to microbial mats.

Sedimentary environment

The facies analyses for the study area suggest that during the Middle to Late Miocene, sedimentation took place in a mudflat-saline lake complex (Fig. 7) similar to that described by Calvo *et al.* (1995) and Calvo *et al.* (1999) for correlatable dolomite deposits in the Madrid Basin. Similarly, the tabular bedded dolomite is interpreted as open lake deposits. According to the regional sedimentary model established by Armenteros (1991), and considering the thickness along with the associated features of the dolomite beds, the lake can be characterized as a shallow saline lake. The scarcity of detrital grains in the facies is indicative of a low-energy environment, almost devoid of clastic inputs. Dolomite with gypsum rosettes and silica facies may have formed in the saline mudflat-marginal lake sub-environment where sub-aerial exposure conditions alternated with flooding episodes (Fig. 7). Dolomite beds containing authigenic sepiolite and palygorskite probably deposited in ponds and marshes which extended to the mudflat areas of the lake characterized by very low surface slopes (Calvo *et al.*, 1999).

PETROGRAPHY AND COMPOSITION OF DOLOMITE

The dolomite beds are mainly structureless or they show laminated to shrub microfabrics. The two latter structures produce a bindstone fabric, typical of stromatolites.

One type of dolomite microfacies consists of bindstone, characterized by crenulated dolomicrite laminae less than 1 mm thick with

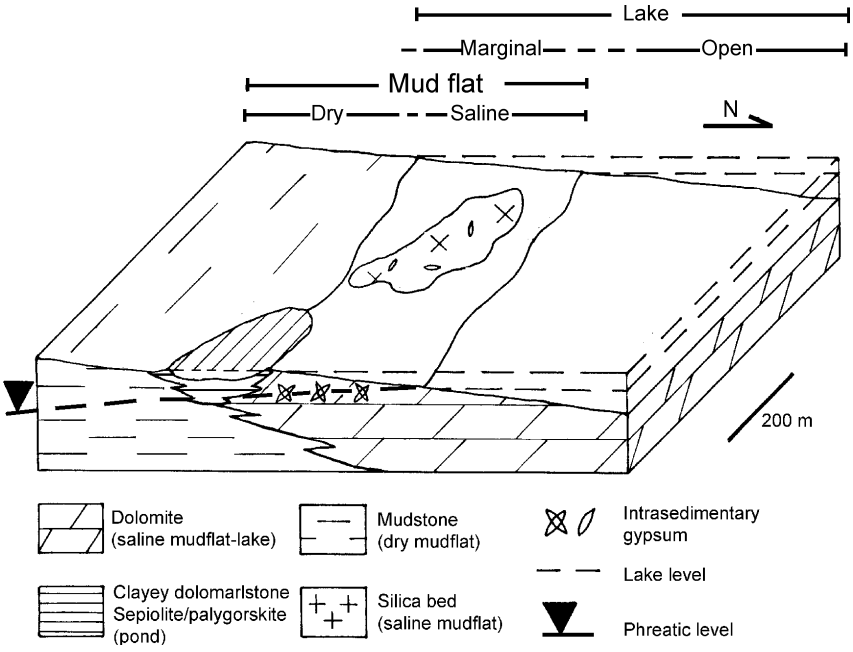

Fig. 7. Schematic diagram illustrating the depositional model with associated facies of the study area.

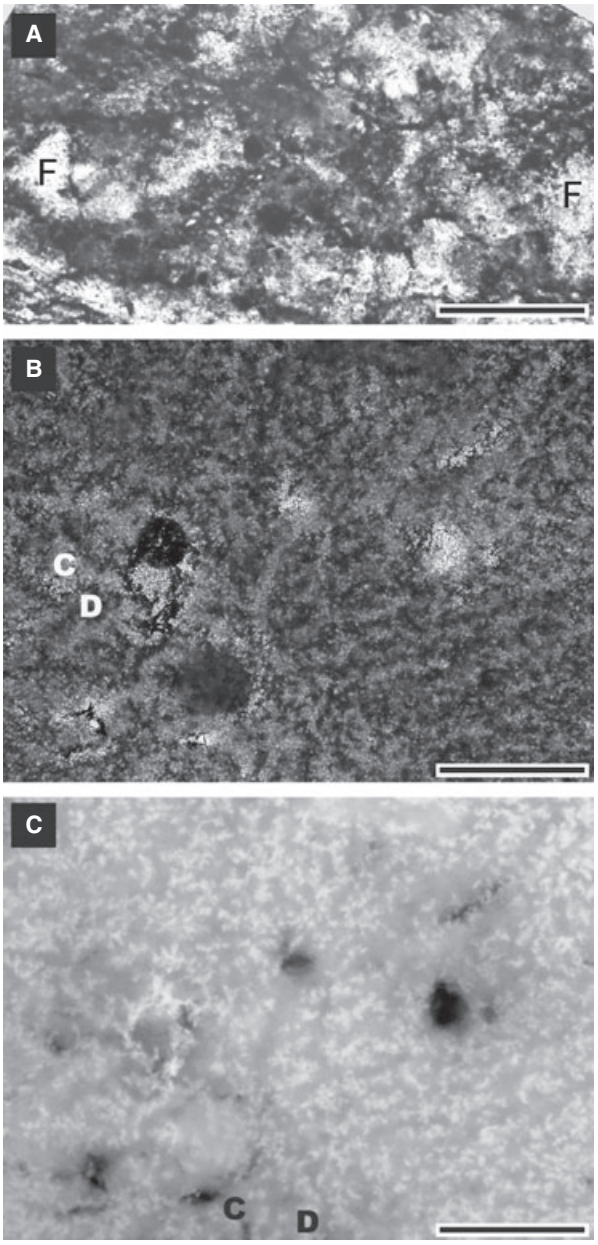

Fig. 8. Thin-section photomicrographs of dolomite microfacies. A: Dolomite clots and filaments and fenestral pores (F) cemented by calcite. Scale bar 75 μm. B: Irregular morphologies of densely packed dolomite shrubs. (D) Dolomite, (C) calcite. Scale bar 150 μm. C: the same as B but under UV fluorescence. Note dolomite shrubs all fluoresce, whereas the surrounding calcite spar does not.

dolomite clots and dispersed silt-size detrital particles (Fig. 8A). As highlighted by fluorescence microscopy, the laminae have a yellow fluorescence, which indicates the presence of light hydrocarbons within the laminae (Chafetz & Guidry, 1999). Sub-millimetre size fenestrae filled by calcite and/or silica are fairly common between the micrite. Interspersed calcite bioclasts of molluscs, ostracods and hemispherical colonies of filaments occur occasionally in the laminae. Commonly, the laminar arrangement is disrupted by burrow bioturbation. Burrow traces up to a few millimetres in diameter are cylindrical in shape. These traces are identifiable by meniscated-backfill structures composed of dolomicrite and/or silica and minor silt-size quartz, mica and feldspar clasts.

Accessory barite is ubiquitous in dolomite beds, especially in those with gypsum moulds. In general, the barite up to 100 μm in size exhibits tabular habits, not easily recognizable due to intense corrosion with carbonates (Sanz-Montero *et al.*, 2006b). Small percentages of SrO (lower than 5% wt) have been detected rarely in the barite crystals. In addition, up to 50 μm amorphous concretions of apatite occur as an accessory mineral in the dolomite. On the basis of its constituents (carbonate-fluor-apatite), the apatite may be characterized as francolite.

A second type of microfacies often associated with laminar bindstone, consists of dolomite shrubs which have branches splaying from a central point or stem (Fig. 8B). Shrubs range in size, morphology and packing within small areas. Shrubs are made of enchained dolomite crystals which contain variable amounts of C, as revealed by the fluorescence they emit (Fig. 8C) and by EMP and EDS analyses. Shrubs can be encased by calcite crystals which range in size and morphology, but frequently show rounded edges and dendritic arrangements (Sanz-Montero *et al.*, 2005). Growth-framework porosity is scarce in densely packed shrub fabrics. In contrast, this porosity abounds in loosely packed fabrics and may be empty or infilled by calcite.

Under SEM, the texture of the dolomite from both microfacies is characterized by open clusters of up to 5 μm crystals in which a variety of poorly crystallized morphologies can be recognized (Fig. 9). Specifically, dolomicrite crystals result from the aggregation of smaller sub-micrometre crystals. The sub-crystals typically show platelet, ring and rod shapes. In addition, the crystals pervasively include fibrils (Fig. 9A). Separation between contiguous crystals is also spanned by organic strands and fibrils which contain variable amounts of C, Si, Mg and Ca, as revealed by EDS microanalyses (Fig. 10).

In many cases, dolomicrite has distinctive spheroid hollow cores (see Fig. 9B). These crystals consist of an arrangement of thin dolomite platelets around the core which usually have

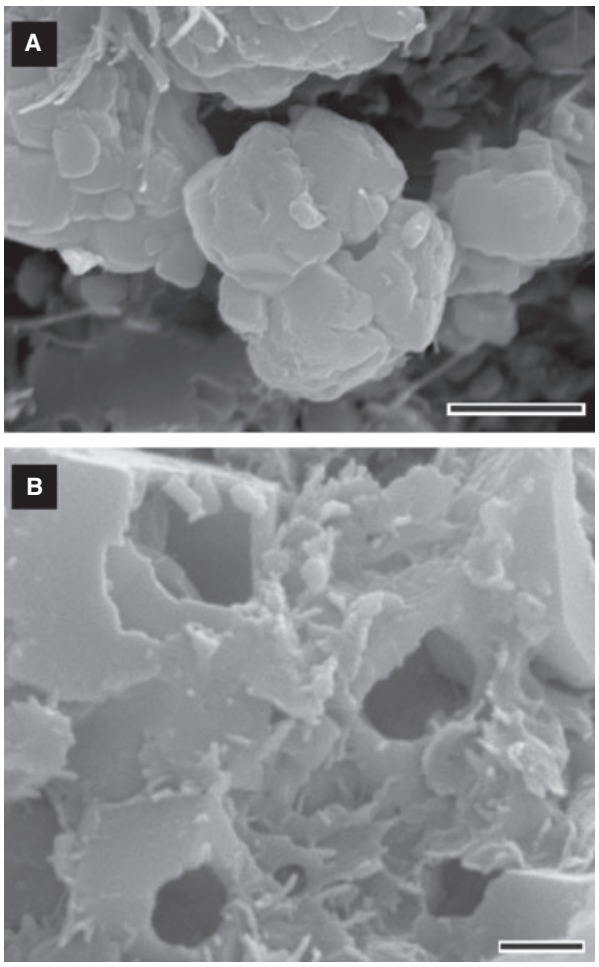

Fig. 9. SEM photographs of freshly broken samples. (A) Openly packed dolomite crystals result mostly from the aggregation of thin platelets. Note poorly crystallized morphologies, and the abundance of intracrystalline porosity and fibrils (recognizable in the upper left corner). Scale bar 2 μm. (B) Dolomicrite exhibiting inner spheroid holes with an array of platelets around them. Scale bar 1 μm.

rhombohedral terminations towards the edges. Frequently, the dolomicrite aggregates occur embedded in Mg-Si-C-rich substances (Fig. 11), which also contain variable amounts of Ca, Al and S, and minor Fe. Locally, C-rich non-crystalline spheroids in the same range of sizes, morphologies and arrangement as dolomicrite grains are also discernible (Fig. 11), their composition and arrangement indicate that embedding substances may represent mineralized remains of mucus and extracellular polymeric secretions (EPS), which typically embed the microbial communities in mats and biofilms (Arp *et al.*, 1999; Westall *et al.*, 2000; Decho *et al.*, 2005). EPS may be desiccated giving rise to unstructured fibrils and deflated films (Renaut *et al.*, 1998), similar to those linked to dolomicrite clusters. Fibril and EPS remains are widespread in Miocene dolomite stromatolites from the Madrid Basin described by Sanz-Montero *et al.* (2006c).

Mineralogical and stable isotope results obtained for the different dolomite facies are summarized in Table 1. Mineralogical analysis reveals that the degree of ordering in the dolomite samples, determined by measurement of indices 015 and 110 from X-ray traces, ranges from 0·20 to 0·64 (averaging 0·48). These values indicate that the dolomites are poorly ordered (Kinsman, 1964). According to the mol.% $CaCO_3$ values determined in the dolomites (48·7 to 55·5 mol.% $CaCO_3$, averaging 52·81%), these can be characterized as slightly Ca-rich, thus, they are non-stoichiometric. Molar ratios obtained from EMP analyses also show that most dolomite samples are enriched in Ca. Dolomite beds deposited in the open lake sub-environment are more calcic than those precipitated in the lake margin (see Fig. 7).

It is generally assumed that poorly ordered non-stoichiometric dolomite is susceptible to recrystallize to nearly stoichiometric and better ordered crystals. Isotopic signatures, especially $\delta^{18}O$, can also be expected to change during burial (Tucker & Wright, 1990). However, the Miocene dolomites are calcic, poorly ordered and show non-planar shapes. Likewise, the dolomicrite forms loosely packed aggregates that exhibit high intercrystalline and intracrystalline porosity rates (see Fig. 9). These features, along with the lack of induration of the dolomite beds, allow the authors to exclude that the dolomite has undergone significant recrystallization. Consequently, the isotope data are considered to be indicative of the sedimentary fluids.

The isotopic composition of the dolomite samples is characterized by negative values for carbon, $\delta^{13}C_{PDB}$ ranging from −6·38‰ and −1·41‰, averaging −4·17‰. In contrast, the $\delta^{18}O$ values oscillate within a narrower range, $\delta^{18}O_{PDB}$ ranging from −1·33‰ and +2·81‰, average +0·60‰ (Table 1, Fig. 12). Dolomite beds precipitated in the open lake sub-environment display both the less negative values for carbon and the more positive values for oxygen. On the other hand, marginal dolomite deposits that occur associated with silica or gypsum are more enriched in ^{12}C. However, dolomite associated with silica is generally characterized by more depleted ^{18}O isotopic signatures than dolomite associated with intrasedimentary gypsum crystals.

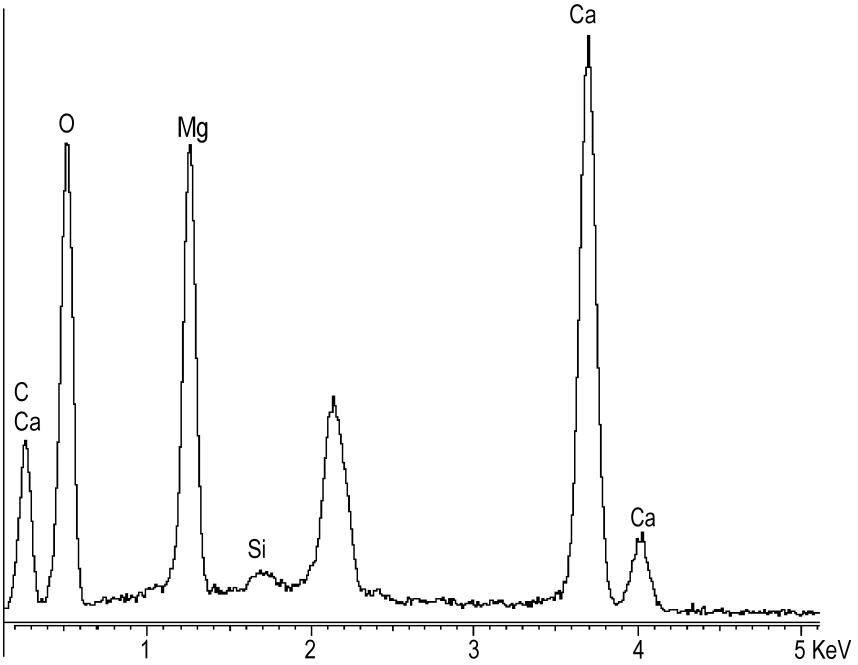

Fig. 10. EDS spectrum showing the typical composition of the dolomite crystals shown in Fig. 9A, with minor amounts of Si. Unlabelled peak at 2·15 KeV corresponds to the gold coating.

PETROGRAPHY AND COMPOSITION OF SILICA FACIES

Two, often associated, microfacies (nodular and laminar) have been differentiated in the silica beds. In mineralogical terms, silica, characterizable as opal CT with minor quantities of quartz, coexists with variable amounts of carbonates (dolomite and scarce calcite), and with scattered detrital quartz, feldspar or mica grains. Sepiolite and palygorskite concentrate as interdigitated thin laminae in some layers.

Nodular microfacies are composed of millimetre to centimetre-size nodules embedded in silica. The nodules consist mainly of luminescent dolomicrite with a variety of microfabrics, such as massive, clotted, filamentous, bushy or bioclastic (with moulds of ostracods). Scattered nodules with intrasedimentary gypsum crystals filled by fibrous silica (chalcedony) have been observed in the mixture. The concurrence of micro-nodules, desiccation cracks and bioturbation traces in many of the nodules is indicative of sub-aerial exposure events. Silica embedding the nodules consists of an opal mesh on which rest variable amounts of openly packed dolomite crystals. Dolomite grains luminesce, whereas the opalline matrix does not. Abundant burrow traces extend in all directions and disturb the nodular fabric; they typically show cylindrical backfill structures composed of microcrystalline quartz, dolomicrite and organic matter. Gypsum moulds and pseudomorphs appear disseminated within the infills.

In the laminar microfacies 2 to 10 mm thick discontinuous layers alternate showing micronodular, micro-laminated and massive fabrics. Burrow tubes, which are not so densely distributed as in the nodular microfacies, have been observed disrupting the layered micro-structure. The three types of fabrics are composed of variable mixtures of dolomite and opal CT, with minor calcite and detrital clasts. Occasionally, Fe-oxides after pyrite have been recognized in the groundmass.

Petrographic analyses of the silica matrix, especially in laminar microfacies, show distinctive micro-structures attributable to microbial mats or biofilms, i.e. densely entangled thin layers of micro-organisms glued together by EPS and other metabolic products (Westall *et al.*, 2000). The ubiquitous presence of C in the laminar microfacies, as detailed below, reinforces the microbial interpretation. Figure 13 shows the typical aspect of silicified biofilms, characterized by a multi-layered structure, frequently microfolded, where filaments, bacteria, other collapsed microbes and fibres coexist, fused together and impregnated by silica. Dehydratation and curling of the edges give a flaky appearance to the films. Fenestrae porosity, a few micrometres in size, is frequently observed in the biofilm. The edges of the fenestrae are serrated, which gives rise to sub-triangular to sub-rhomboid shaped pores

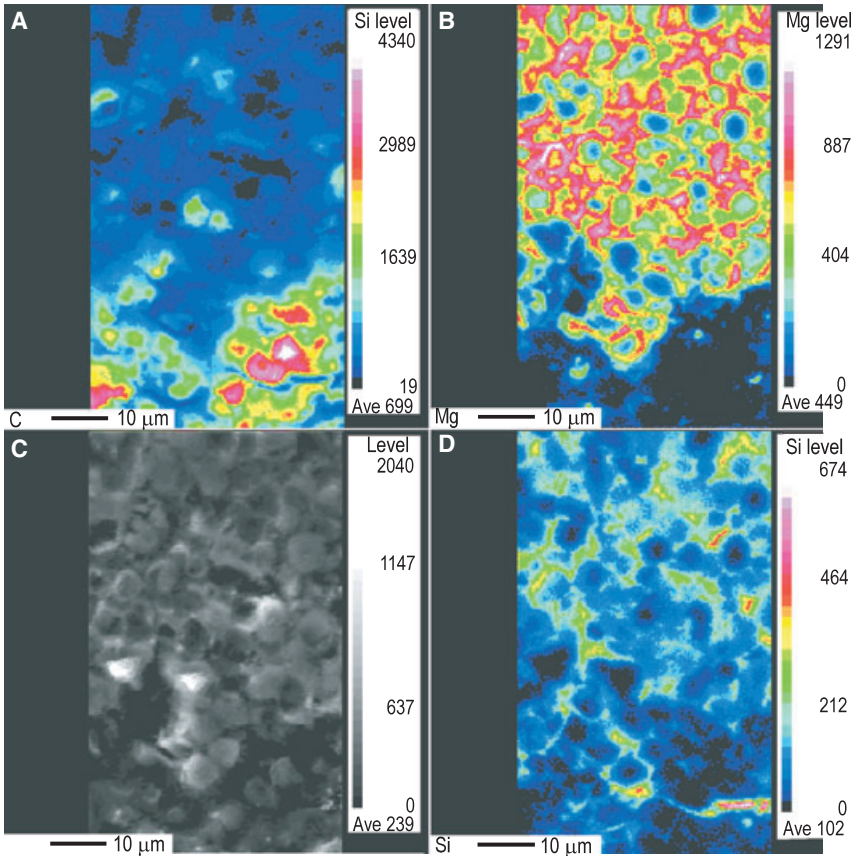

Fig. 11. Elemental mapping with the electron microprobe technique showing the content variations of C (A), Mg (B) and Si (D) in dolomite and C-rich spheroids which are embedded in a substance enriched with C-Mg-Si, possibly EPS (C, SEM photograph). Non-mineralized structures enriched in C are mainly concentrated in the lower part of the images and become progressively mineralized in the upper part. The Si content is irregularly distributed but it is significantly higher in the embedding matrix. The highest levels of Mg are observed in spheroid dolomite crystals, although significant quantities of Mg are also present in the surrounding substances which are not dolomite.

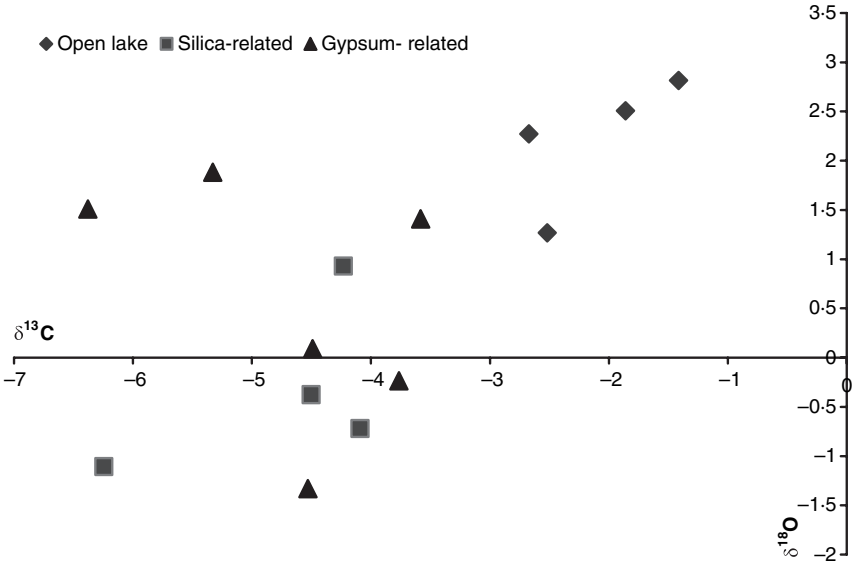

Fig. 12. Plot of $\delta^{18}O$ versus $\delta^{13}C$ for dolomite beds deposited in the sub-environments of open and margin lakes, associated with silica or with gypsum deposits. Values are reported in permil relative to PDB standard.

(Fig. 13B and C). The presence of these pores is punctuated by significant concentrations of dolomicrite inside or in their vicinity (Figs 13C,D and 14A). Rather more dispersed dolomite crystals are observed throughout the biofilm and always have a close attachment to the substrate, whose fibrillar structure is closely imitated by the basal faces of dolomite (Figs 13D and 14B,F). Specifically, dolomite crystals are similar to those described for dolomite beds. Thus, typical micrite-size crystals result from the aggregation of thin platelets which seem to be arranged in accordance with the

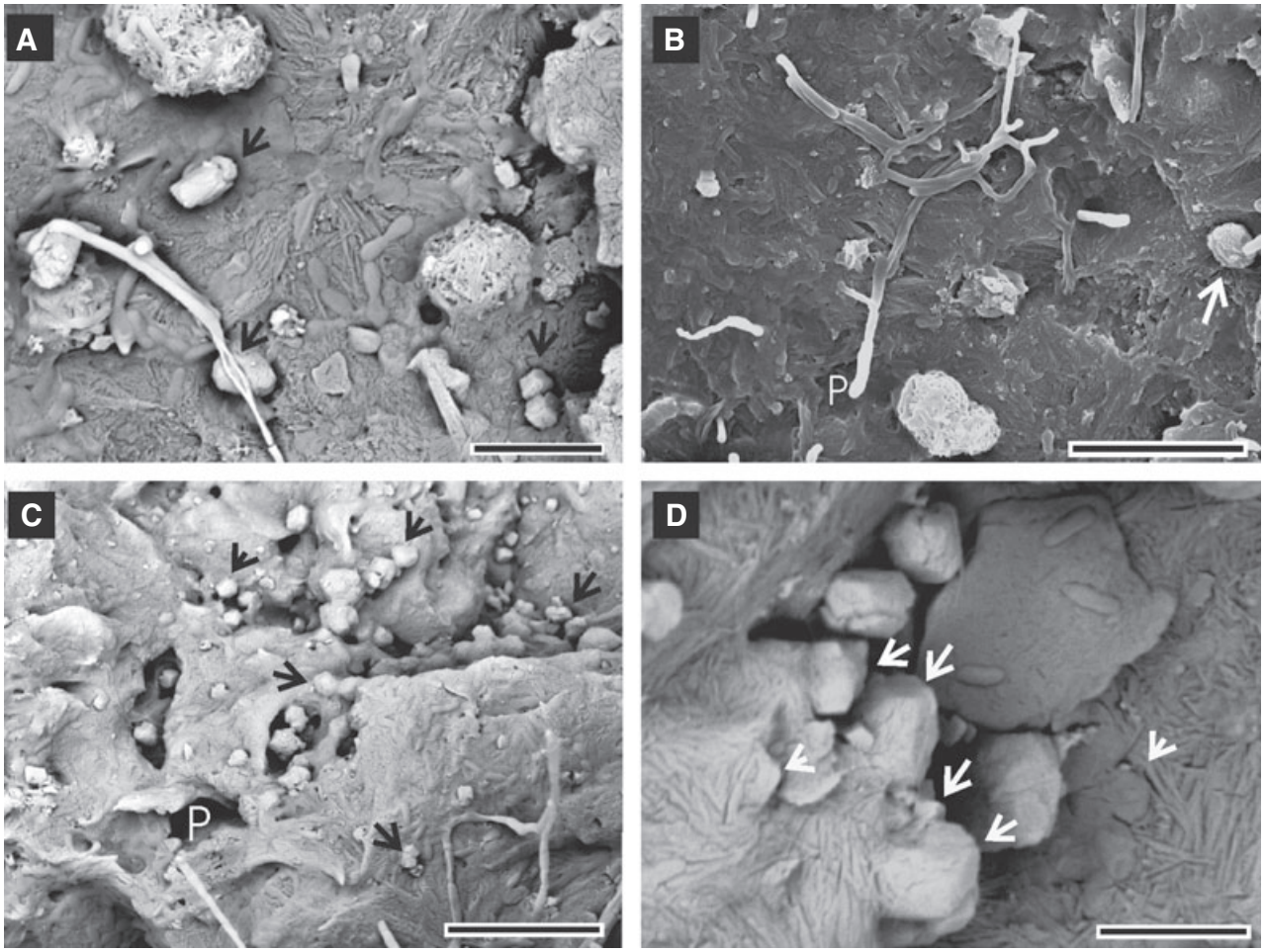

Fig. 13. SEM images of silica biofilms, characterized by the presence of filaments, bacteria and other collapsed microbes, and fibres, fused together by mucus and impregnated by silica. Some dolomite grains resting on the silica template are arrowed. The photographs were taken using the backscattered electron operation mode, except (B). (A) Typical view of silica biofilm showing filaments, bacillus-like microbes and fibrillar EPS. Notice dolomite crystals scattered on the substrate (arrowed). Scale bar 5 μm. (B) Image of silica filaments on biofilms associated with dolomite (arrowed) and serrated pores (P). Scale bar 10 μm. (C) View of biofilm showing fenestral pores (P) outlined by dolomite crystals (arrowed). Note the serrated morphologies of the pore edges. Scale bar 10 μm. (D) Magnified image of a pore with dolomicrite crystals (arrowed) intimately fixed to the silica substrate. Note that the silica–dolomite interface is not sharply defined. Instead, the surface of the dolomite crystals resting on the silica mimics the fibrillar arrangement of the substrate. A detached fragment of the silica biofilm to the upper right of the image shows some silicified rod-shaped microbes on the top. Scale bar 3 μm.

layered pattern of the biofilm (Fig. 14A and B). Distances between successive crystals are spanned by bridges, and fibrils are ubiquitous in the group.

The Ca content and the degree of order of dolomite associated with silica are in the same range as those found in other dolomite beds (Table 1). Isotopic composition for oxygen is slightly lighter than in other dolomite facies. The $\delta^{13}C$ data coincides with dolomite including gypsum pseudomorphs, also interpreted as marginal facies precipitated in the mudflats during lake expansion stages. Heavier isotope values obtained for oxygen from open lake dolomites are indicative of more concentrated brine water (see Fig. 12).

Thin fibrillar layers which lie horizontally and locally exhibit micro-folding have been interpreted as silicified EPS. Each layer is comprised of closely packed silicified fibres (Fig. 14). These types of fibres or tube-like structures have been also recognized in silicified biofilms by Renaut *et al.* (1998), who attributed their formation to the curling of EPS (mucus). Taken individually, the fibres (sub-micrometre in diameter and averaging 4 μm in length) are straight and, locally, are

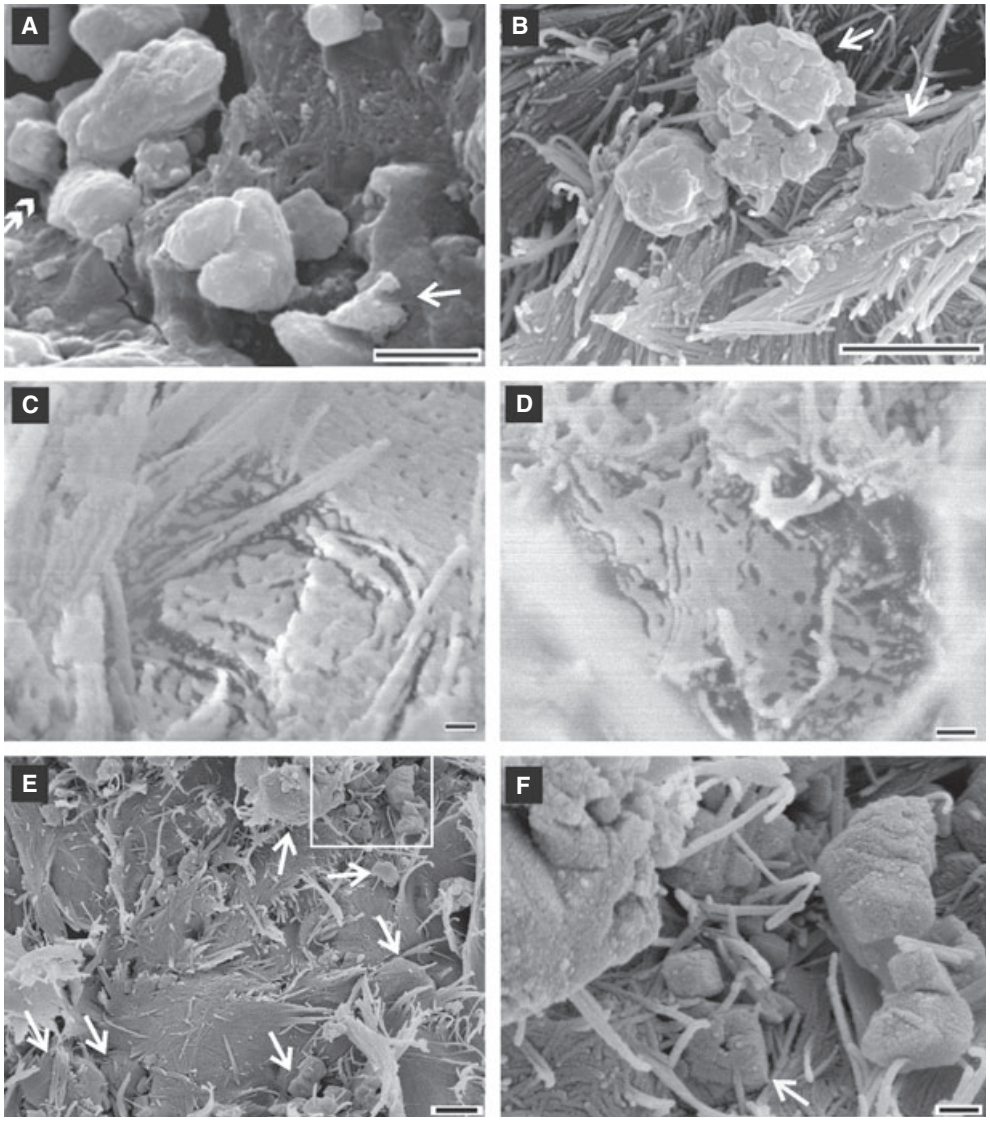

Fig. 14. SEM photographs of dolomite crystals formed on highly structured fibrillar templates (EPS). (A, B) SEM photographs. (C–F) field emission SEM photographs. (A) Dolomite crystals (white crystals) in pores of the silica biofilm. Specifically, dolomite crystals consist of a vertical arrangement of thin platelets which seem to reproduce the layered pattern of the substrate (grey fibres). The distances between adjacent dolomite crystals are spanned by bridges (double-headed arrow). Note the parallelism in the serrated morphologies of the pore and the dolomite outlines. The serrated forms result from the reticular array of the fibre bundles. The dolomite crystals are intricately tied to the substrate as shown in the lower right corner of the picture (arrowed). Scale bar 3 μm. (B) Corpuscles and different sized dolomite crystals (arrowed) are developed on a silicified fibrillar substrate. Scale bar 3 μm. (C) Multi-layered and fibrillar structure of EPS, each layer composed of nanofibres arranged in bundles according to a hexagonal order, typical of opal packing. Chains of nanospheres of opal encrusting the fibres are discernible at this magnification. Scale bar 100 nm. (D) Reticular arrangement of fibres with some angles at approximately 120°, resulting in rhomboid morphologies. Scale bar 100 nm. (E) Mesh of fibres from which scattered groups of dolomite crystals are differentiated (arrows). Scale bar 1 μm. (F) High magnification of (E). A rhombohedral dolomite crystal grown epitaxially on the fibrillar substrate is observable in the centre (arrowed). Scale bar 200 nm.

curved at the end giving rise to walking stick shapes. Fibres occur encrusted with nanospheres of opal (Fig. 14C). The packs of fibres are arranged according to a reticular fabric, with intersection angles of approximately 120° and 60°, typical of the hexagonal to trigonal crystallographic system (Fig. 14C and D). The ordered configuration of the mineralized substrate provides a suitable template for the development of rhomboid and rhombohedral forms which are, in many cases,

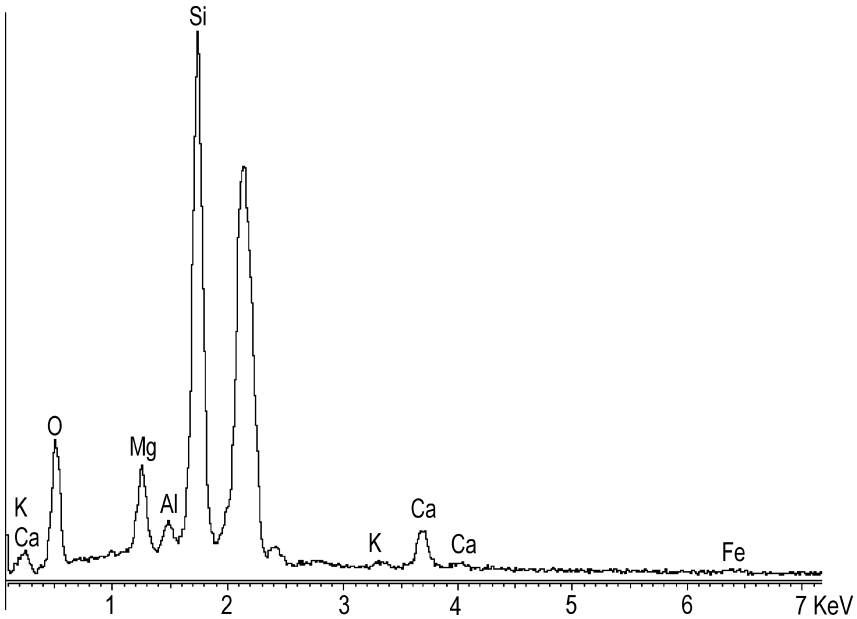

Fig. 15. EDS spectrum showing the composition of silica fibres. Unlabelled peak at 2·15 KeV corresponds to the gold coating.

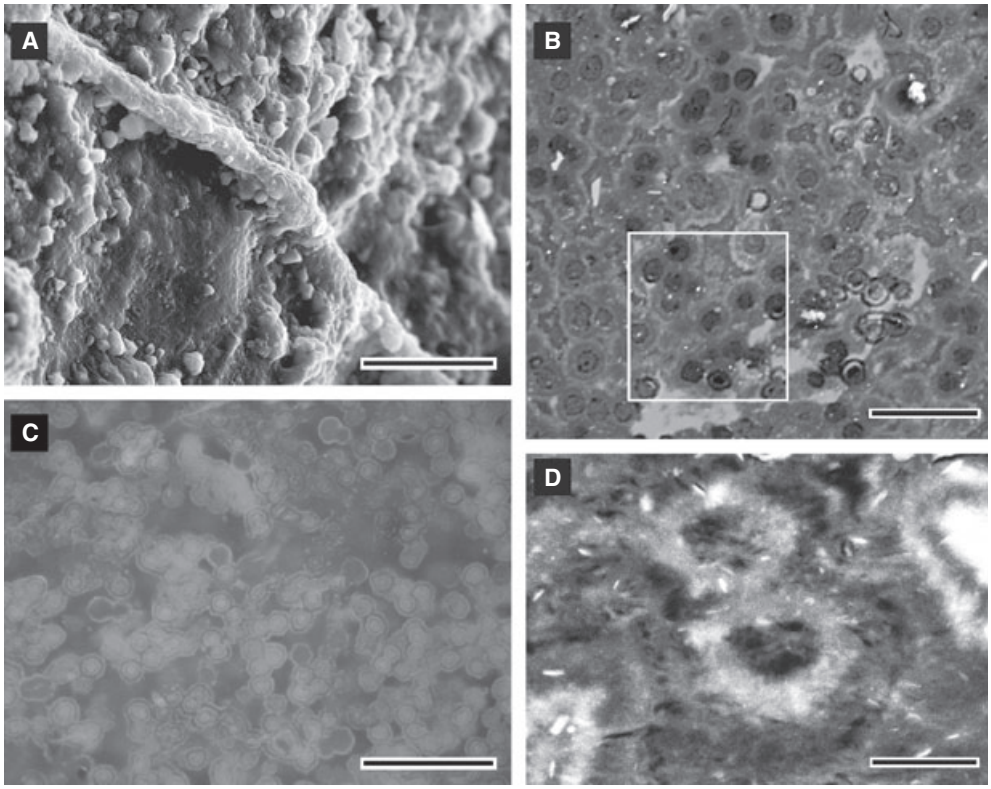

Fig. 16. Photomicrographs illustrating the characteristics of silica filaments and coccoid cells. (A) SEM photograph of a filament lying on a silica biofilm. The collapsed filament is encrusted with dolomite crystals. Scale bar 15 μm. (B) SEM–BSE image showing the arrangement of the silicified clusters of coccoid cells embedded by silica EPS. The cells consist of a dark core and a grey envelope. Additionally, a whitish envelope surrounds a group of cells. The silica matrix ranges in colour from grey to white. The squared area is magnified in Fig. 17. Scale bar 40 μm. (C) UV fluorescence photomicrograph showing the luminescence of the well-preserved cell clusters and the lack of luminescence in the matrix. The presence of a core, an envelope, and a sheath surrounding groups of cells is also discernible under fluorescence. Scale bar 75 μm. (D) SEM–BSE view illustrating the structure of the cells which includes a core with granular remains, an individual envelope, and a common sheath with a fibrillar structure. Scale bar 5 μm.

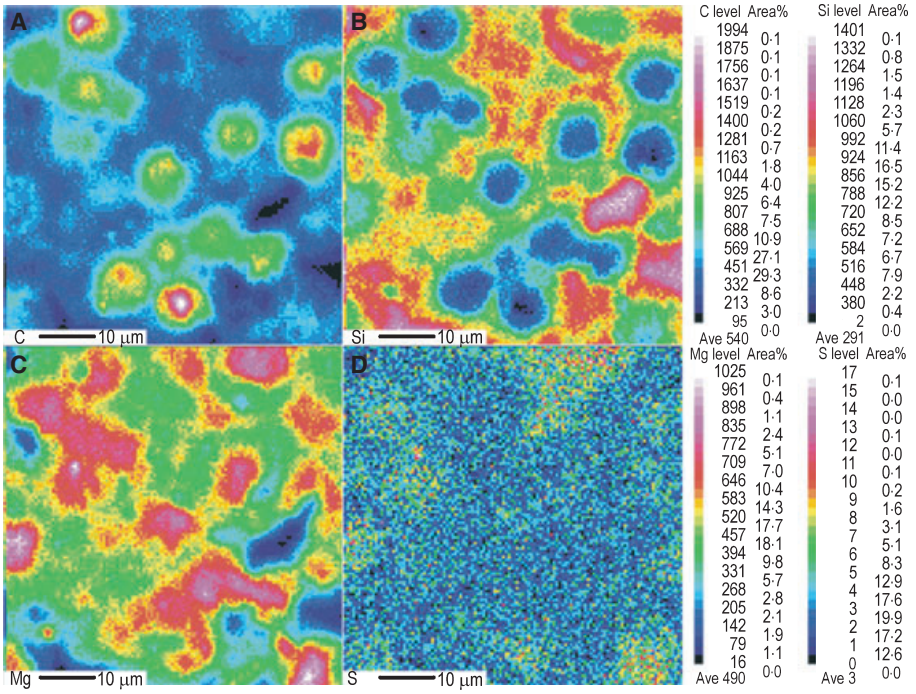

Fig. 17. Elemental mapping with the electron microprobe technique showing the content variations of C (A), Si (B), Mg (C) and S (D) in the silicified cell clusters squared in Fig. 16B. Si fixation mainly takes place in the matrix (EPS) embedding the cells. Si values decrease gradually towards the core of the cells. The inverse trend is observed in the C and Mg values. The highest values of S correlate positively with the highest values of Mg in the core of the coccoids.

mineralized in dolomite (Fig. 14E and F). Frequently, the resulting crystals reproduce the fibrillar appearance of the substrate, with fibres shared by contiguous crystals (Fig. 14E and F). Fibres are generally composed of Si with variable percentages of Mg, and minor amounts of Ca, Al, Fe, C and K (Fig. 15) as revealed by several spot analyses using an EDS on the SEM and other analyses with the EMP technique.

Two main types of silicified micro-organisms have been identified: those with filamentous forms and those with coccoid forms (see Figs 13A,D, 16 and 17). Filaments occur as open tangle networks resting on the silicified biofilms. These filaments are encrusted with dolomite platelets and/or impregnated with massive silica (Fig. 16A); they can be several micrometres in length and less than 4 μm in diameter. Some examples of branching were found locally. Filaments occur partially or totally collapsed. Like fibres, filaments are mainly composed of Si, C, Mg and Ca, and, to a lesser extent, Al and Fe.

Silicified clusters of coccoid cells abound typically in the stromatolites showing pustular morphologies (see Fig. 4B), and occur as microscopic groups composed of equidimensional spherical, irregularly arranged cells, embedded in a silica matrix (probably EPS) (see Fig. 16B to D). Cell units are up to 12 μm, including a core of up to 7 μm in diameter and an envelope which varies greatly in thickness. Apart from their own envelope, the cells can share an additional envelope with a group of two or more individuals. The cells frequently contain granular material which, like envelopes, is highly luminescent (see Fig. 16C); this indicates the presence of organic matter, which is also corroborated by spot analysis by EDS and EMP. The precise distribution of C, Si, Mg and S throughout a cluster of cells embedded in a silica matrix has been obtained by the digital mapping shown in Fig. 17. According to spot quantitative analyses obtained by the EMP technique, the lowest values of SiO_2 (31% wt) are measured in the luminescent cell cores containing granular material (see Fig. 16C); however, they have the highest values of MgO (8% wt) and CO_2. The sum of the oxides in the analyses is low at 58%, this value is assumed to be mostly the CO_2 content, and is not measurable by the EMP. In addition, CaO is absent or appears in very low percentages (0·1% wt). In contrast, in silicified non-luminescent cores, the SiO_2 content reaches 80% wt, and the MgO percentages are lower than 3% wt.

In the individual luminescent cell envelopes the values of SiO_2 increase up to 62% wt, the CO_2

and MgO (6%) decrease in comparison with the cell core. In the second envelope, covering several cells, the SiO_2 content is higher than in the individual ones (65% wt) and, consequently, lower in CO_2 and MgO. In a few cases, some dolomite crystals are precipitated in this envelope. The silica matrix surrounding the cell clusters does not luminesce and displays low values of CO_2 and MgO (lower than 4%) and high values of SiO_2 (75%). The S is distributed irregularly in the group (Fig. 17), although it tends to correlate positively with C and Mg. Other elements such as Al, Fe and K are also found in the group and are associated with detrital feldspar and mica grains.

DISCUSSION AND INTERPRETATION

Microbial precipitation of dolomite

Based on the lack of evidence of any carbonate precursor, and sedimentological, geochemical, mineralogical and textural features reported here, Miocene dolomite from the Duero Basin has been interpreted as a primary mineral phase. Dolomite formed through microbial-mediated processes which took place in microbial mats and biofilms. The micro-structure of the microbial mats has been preserved in microlamination and shrub fabrics. Features of spheroid-shaped organic remains associated with dolomite, including composition, size, morphology, and organization make it possible to interpret them as related to the growth of microbial colonies and, in particular, of coccoid cyanobacteria. Coccoid taxa coexist with other microbial forms, all with embedded extracellular polymeric substances and mucus, as documented regarding modern microbial mats (Noffke *et al.*, 2003). Figure 11 shows how most of the preserved coccoid cells appear mineralized in dolomite. Isotopically, the dolomite crystals are significantly enriched by ^{12}C, which supports the incorporation of organically derived carbonate ions in the mineral. On the other hand, $\delta^{18}O$ values of dolomite oscillate within a shorter range, indicative of slight variations in the saline conditions of the water from which dolomite precipitated.

In general, the textural, compositional and structural features of the dolomite resemble those described by Vasconcelos & McKenzie (1997) and Wright (1999) from modern lakes, where microbially mediated dolomite is forming. In the environments described by those authors dolomite precipitates as a poorly crystallized mineral. Similar to the dolomites studied in the Miocene lake deposits of the Duero Basin, dolomite sediments from the above-mentioned modern lakes, in particular those analysed by Vasconcelos & McKenzie (1997), are typically formed from Ca-rich dolomite.

The range of environmental conditions conducive to biologically mediated formation of dolomite in recent deposits was expanded from coastal areas (Vasconcelos & McKenzie, 1997; Wright, 1999) to inland saline lakes (Corzo *et al.*, 2005). Moreover, the occurrence of microbial dolomites in the geological record has been recognized on the basis of fossilized bacteria, crystal textures, isotopic values and other biomarkers (García del Cura *et al.*, 2001; Rao *et al.*, 2003; Sanz-Montero *et al.*, 2006c).

Influence of the organic matter decay

In Miocene dolomite beds only some fibrils interpreted as remains of deflated extracellular polymeric secretions (EPS) are preserved. Silicification processes probably protected the EPS against significant degradation, and prevented major dolomite formation. Only a few dolomite crystals resting on silicified EPS were formed, and these mainly occur in the vicinity of alveolar pores, which probably originated through organic matter decay. The concentration of dolomite crystals in the margin areas of mucus shows that the decomposition of organic material may have favoured dolomite nucleation. In non-silicified areas, mats have been interpreted as being completely decayed, which led to the massive precipitation of dolomite forming continuous dolomite beds. In modern microbial mats, decomposition of organic material is the main process leading to carbonate precipitation (Noffke *et al.*, 2003). Additionally, Vasconcelos *et al.* (1995) and Vasconcelos & McKenzie (1997) proposed a model for dolomite formation, in which the photosynthetically produced organic matter can be recycled microbially by sulphate-reducing bacteria. Laboratory experiments conducted in parallel have shown that the formation of dolomite can be due to microbial sulphate reduction (Van Lith *et al.*, 2003; Wright & Wacey, 2005). The bacterial sulphate reduction processes may overcome the kinetic barrier to dolomite formation by increasing pH and carbonate alkalinity (Warthmann *et al.*, 2000). In addition, Moreira *et al.* (2004) suggested that sulphide oxidation also plays a role in the

precipitation of dolomite in the Brejo do Espinho lagoon, Brazil. In the lagoon sulphide oxidation may be mediated by microbial communities, in which the H_2S produced by sulphate reducers may fuel the sulphide-oxidizing bacteria. These micro-organisms may further promote dolomite precipitation by providing charged nucleation sites. Thus, it may be the coupling between oxidation and sulphate reduction that produces the chemical conditions necessary for dolomite precipitation. This view, considering dolomite as the result of symbiotic interactions, is coherent with the stratificated structure of microbial mats, in which a dynamic association of micro-organisms affects local geochemistry with consequences for mineralogy of the local environment (Douglas, 2005; Visscher & Stolz, 2005; Vasconcelos *et al.*, 2006). In Miocene dolomites the ubiquitous presence of sulphur, barite and iron oxides after pyrite suggests that the formation of dolomite may have been related to the metabolic activity of bacteria under both sulphate-reducing and sulphide-oxidizing conditions. Pyrite formed as a by-product of the sulphate-reducing processes (Machel, 2001). The occurrence of barite is also considered to be related to pH and redox changes during the microbially mediated formation of dolomite (Sanz-Montero *et al.*, 2006b).

Influence of the binding capability of EPS

The capability of EPS which are produced by cyanobacteria in microbial mats, to bind and concentrate Ca and Mg, carbonates, silica and other ions from the surrounding water has been recorded in various papers (Konhauser, 1998; Sánchez-Navas *et al.*, 1998; Folk & Chafetz, 2000; Léveillé *et al.*, 2000; Westall *et al.*, 2000; Arp *et al.*, 2003; Van Lith *et al.*, 2003; Decho *et al.*, 2005; Souza-Egipsy *et al.*, 2005). Like those described in modern environments, EPS preserved in Miocene samples, apart from Si, fixed Ca, and, Mg, in higher concentrations. Souza-Egipsy *et al.* (2005) suggested that the different affinity for Mg^{2+} between cyanobacteria and other bacteria due to differences in the size and cell wall structure, enhances the fossilization potential of the cyanobacteria in Mono Lake, USA. Thus, bacteriolysis of cyanobacterial biomass may have promoted dolomite growth by increasing the concentration of Mg released from decaying Mg-enriched exopolymers.

Additionally, Mg^{2+} and Ca^{2+} are the main ions bound to the outer membrane of some bacteria (Coughlin *et al.*, 1983), thus creating suitable environments for the precipitation of dolomite around the living cells. According to Sanz-Montero *et al.* (2006c), this process accounted for the formation of dolomite crystals with rounded cores forming Miocene dolomite beds from the Madrid Basin, with globular holes representing the former sites of microbial occupancy.

Influence of the structure of the organic template

The general structure of polymeric substances is not discernible, except in the beds where these occur silicified. Silicified EPS consist of fibrillar layers, arranged in accordance with a reticular fabric, in which angles of intersection at approximately 120° and 60°, typical of the hexagonal to trigonal crystallographic system, have been frequently observed (Fig. 14). The ordered configuration of the mineralized EPS seems to provide a suitable substrate for the development of rhomboid and rhombohedral forms, which may be mineralized in dolomite. Frequently, the resulting crystals include fibres of EPS. Similarly, certain organic compounds of mucus were reported to be locked in or even preferentially absorbed by the growing crystals of carbonates in microbialites forming in Pyramid Lake (USA) (Arp *et al.*, 1999).

The paracrystalline character of the proteinaceous layers which forms the surface of some groups of cyanobacteria cells has been recognized by Schultze-Lam *et al.* (1992) and Schultze-Lam & Beveridge (1994). The latter have shown that this layer can act as a nucleation site for calcite and other minerals. Similarly, Arp *et al.* (1999) concluded that Pleistocene 'tufa' fabrics may reflect the reticular structure of the EPS in which microsparite precipitated. Dupraz *et al.* (2004) also concluded that random carbonate precipitation can result from highly organized macromolecules, of EPS, in microbialites developed in a hypersaline lake, Bahamas. According to Dupraz & Visscher (2005), alteration of EPS yields reorganization of acidic sites in templates that allows $CaCO_3$ precipitation. In addition, through the study of synthetic systems, Mann *et al.* (1993) have highlighted the importance of electrostatic binding, geometric matching (epitaxis), and others, in molecular interactions at inorganic to organic interfaces. In general, the effect of the organic template is to lower the activation energy of nucleation. Accordingly, templated dolomite formation may be viable under earth surface conditions.

Silica precipitation in organic templates

In Miocene samples, the exceptional preservation of cell membranes and EPS ultrastructures indicate that a silicification process in microbial mats took place very early (Renaut *et al.*, 1998; Konhauser *et al.*, 2001), and may have been favoured by the ability of EPS to bind Si (Westall *et al.*, 2000; Souza-Egipsy *et al.*, 2005). The nucleation of silica on organic templates has been documented to be of crucial importance in experimental investigations (Konhauser *et al.*, 1993), and could result from the formation of hydrogen bonds between organic compounds with residual surface charges and silicic acid (Westall *et al.*, 1995) or the sorption of negatively charged silica ions to positively charged surface functional groups (Urrutia & Beveridge, 1993). Whether the fixation of silica on organic matter was a passive process (Westall *et al.*, 1995) or biologically mediated by cyanobacteria (Konhauser *et al.*, 2001) is often controversial in the geological record (Mukhopadhyay *et al.*, 2004). In the case reported here, the exceptional preservation of membranes and ultrastructure of cyanobacteria, with some of them apparently having been fossilized during the phase of cell division, suggest a passive enclosure of micro-organisms.

Polymeric fibres of Miocene biofilm might have further templated the nucleation of the opal nanospheres, providing a hexagonal surface geometry similar to that of the silica precipitates. Brott *et al.* (2001) observed an ordered array of silica nanospheres deposited onto nanopatterned polymer substrates at ambient conditions.

The inferred rapid precipitation of silica and the predominance of opal rather than quartz in Miocene stromatolites indicate that the opal formation was possibly encouraged by the evaporation processes. The evaporation mechanisms provide the high concentrations of silica in the water and the rapidity required for the precipitation of opal (Bustillo & Bustillo, 2000). Papers by Wopfner (1978) and Ambrose & Flint (1981) suggested that shorelines of regressive lakes were the preferred sites for silica precipitation owing to the high evaporation rates. A similar conclusion regarding littoral and eulittoral location of silicification processes was provided for Palaeogene lacustrine carbonates in the Madrid Basin by Bustillo *et al.* (2002). Such palaeogeographical interpretations are consistent with the deduced formation of the silica beds in marginal areas of the lake in the Duero Basin (Fig. 7). This interpretation is based mainly on the transitional relationships between dolomite and silica beds, the typical pustular mat morphologies preserved in some of the silica facies, the relatively light ^{18}O values for associated dolomite, and the higher density of bioturbation traces in silica than in dolomite beds. Bioturbation tubes create further organic micro-environments suitable for silica nucleation, as described by several authors (Gardner & Hendry, 1995; Bustillo & Bustillo, 2000). The drop in water level in the lake is interpreted as possibly having led to a rapid silicification of microbial mats developed in the marginal fringes which prevented their degradation and the subsequent dolomite precipitation.

CONCLUSION

The microbial mats thriving in Miocene lacustrine systems templated the nucleation of dolomite. The organic substrates favoured dolomite precipitation providing a lattice geometry which has been shown to fit the hexagonal order of dolomite. Furthermore, the organic groups bound different ions, Mg^{2+} among others, which probably guaranteed the Mg/Ca ratio required to form the dolomite crystals. The concurrence of these factors accounted for lowering the free energy barrier to dolomite nucleation.

Dolomite crystals consist of an arrangement of sub-micrometre platelets developed on biofilm surfaces and on the outermost cell surfaces of cocci, the latter generally have rhombohedral habits. Diagenetic evolution of the dolomite succession, which has lasted *ca* 15 Ma and has led to a maximum depth of burial of over 100 m, has apparently not produced major changes in the poorly ordered and non-stoichiometric nature of the mineral; this confirms that microbial imprints can be preserved in the geological record, and validates their use as biomarkers.

Towards the marginal areas of the lake, microbial mats became mineralized in opal, this is probably encouraged by Si fixed on organic substances, the reticular arrangement of extracellular polymeric secretions (EPS), and silica supersaturation due to evaporation. An effect of silicification was the preservation of prior dolomite with no signs of replacement. Thus, organic substrates may have alternately templated the precipitation of dolomite and silica as pH and redox conditions changed.

ACKNOWLEDGEMENTS

This work was supported by Project PR45/05-14165, financed by the Education Board of the Madrid Community. We are grateful to J.C. Sanz for his help with the sampling. The authors thank three anonymous reviewers for critically reviewing the manuscript. In addition, Associate Editor John Reijmer and Editor Peter Swart provided valuable comments.

REFERENCES

Alonso-Gavilán, G., Armenteros, I., Carballeira, J., Corrochano, A. Huerta, P. and **Rodríguez, J.M.** (2004) Cuenca del Duero. In: *Geología de España* (Coord. J.A. Vera), **6,** 550–556. SGE-IGME, Madrid.

Ambrose, G.J. and **Flint, R.B.** (1981) A regressive Miocene lake system and silicified strandlines in northern South Australia – implications for regional stratigraphy and silcrete genesis. *J. Geol. Soc. Aust.*, **28,** 81–94.

Armenteros, I. (1991) Contribución al conocimiento del Mioceno lacustre de la Cuenca terciaria del Duero, sector Centro-Oriental. Valladolid-Peñafiel- Sacramenia- Cuéllar. *Acta Geol. Hisp.*, **26,** 97–131.

Armenteros, I., Bustillo, M.A. and **Blanco, J.A.** (1995) Pedogenic and groundwater processes in a closed Miocene basin (northern Spain). *Sed. Geol.*, **99,** 17–36.

Armenteros, I., Corrochano, A., Alonso-Gavilán, G., Carballeira, J. and **Rodríguez, J.M.** (2002) Duero basin (northern Spain). In: *The Geology of Spain* (Eds W. Gibbons and M.T. Moreno), **13,** 309–315. The Geological Society, London.

Arp, G., Thiel, V., Reimer, A., Michaelis, W. and **Reitner, J.** (1999) Biofilm exopolymers control microbialite formation at thermal springs discharging into the alkaline Pyramid Lake, Nevada, USA. *Sed. Geol.*, **126,** 159–176.

Arp, G., Reimer, A. and **Reitner, J.** (2003) Microbialite formation in seawater of increased alkalinity, Satonda Crater Lake, Indonesia. *J. Sed. Res.*, **73,** 105–127.

Brott, L.L., Naik, R.R., Pikas, D.J., Kirkpatrick, S.M., Tomlin, D.W., Whitlock, P.W. Clarson, S.J. and **Stone, M.O.** (2001) Ultrafast holographic nanopatterning of biocatalytically formed silica. *Nature*, **413,** 291–294.

Bustillo, M.A. and **Bustillo, M.** (2000) Miocene silcretes in argillaceous playa deposits, Madrid Basin, Spain: petrological and geochemical features. *Sedimentology*, **47,** 1023–1037.

Bustillo, M.A., Arribas M.E. and **Bustillo, M.** (2002) Dolomitization and silicification in low-energy lacustrine carbonates (Paleogene, Madrid Basin, Spain). *Sed. Geol.*, **151,** 107–126.

Calvo, J.P., Jones, B.F., Bustillo, M., Fort, R., Alonso Zarza, A.M. and **Kendall, C.** (1995) Sedimentology and geochemistry of carbonates from lacustrine sequences in the Madrid Basin, Central Spain. *Chem. Geol.*, **123,** 173–191.

Calvo, J.P., Blanc-Valleron, M.M., Rodríguez-Aranda, J.P., Rouchy, J.M. and **Sanz-Montero, M.E.** (1999) Authigenic clay minerals in continental evaporitic environments. *IAS Spec. Publ.*, **27,** 129–151.

Calvo, J.P., McKenzie, J. and **Vasconcelos, C.** (2003) Microbially mediated lacustrine dolomite formation: evidence and current research trends. In: *Limnogeology in Spain: A Tribute to Kerry Kelts* (Ed. B.L. Valero-Garcés), *Biblioteca Ciencias*, **14,** 229–251. CSIC, Madrid.

Calvo, J.P., García del Cura, M.A., Sanz-Montero, M.E. and **Pozo, M.** (2004) Bacterially induced formation of lacustrine dolomite in Middle Miocene deposits of the Madrid Basin, central Spain. *23rd IAS Meeting of Sedimentology*, Abstract Book 76, Coimbra, Portugal.

Chafetz, H.S. and **Guidry, S.** (1999) Bacterial shrubs, crystal shrubs, and ray-crystal shrubs: bacterial vs. abiotic precipitation. *Sed. Geol.*, **126,** 57–74.

Corzo, A., Luzon, A., van Bergeijk, S.A., Mata, P. and **García de Lomas, J.** (2005) Carbonate mineralogy along a biogeochemical gradient in recent lacustrine sediments of Gallocanta Lake (Spain). *Geomicrobiol. J.*, **22,** 283–298.

Coughlin, R.T., Tonsager, S. and **McGroarty, E.J.** (1983) Quantitation of metal cations bound to membranes and extracted lipopolysaccharide of *Escherichia coli*. *Biochemistry*, **22,** 2002–2007.

Decho, A.W., Visscher, P.T. and **Reid, R.M.** (2005) Production and cycling of natural microbial exopolymers (EPS) within a marine stromatolite. *Palaeogeogr. Palaeoclimatol. Palaeoecol.*, **219,** 71–86.

Douglas, S. (2005) Mineralogical footprints of microbial life. *Am. J. Sci.*, **305,** 503–525.

Dupraz, C. and **Visscher, P.T.** (2005) Microbial lithification in marine stromatolites and hypersaline mats. *Trends Microbiol.*, **13,** 429–438.

Dupraz, C., Visscher, P.T., Baumgartner, L.K. and **Reid, R.P.** (2004) Microbe–mineral interactions: early carbonate precipitation in a hypersaline lake (Eleuthera Island, Bahamas). *Sedimentology*, **51,** 745–765.

Folk, R.L. and **Chafetz, H.S.** (2000) Bacterially induced microscale and nanoscale carbonate precipitates. In: *Microbial Sediments* (Eds R. Riding and S.M. Awramik), pp. 40–49. Springer-Verlag, Berlin.

García del Cura, M.A. (1974) Estudio sedimentológico de los materiales terciarios de la zona centro-oriental de la Cuenca del Duero (Aranda del Duero). *Estudios Geol.*, **30,** 579–597.

García del Cura, M.A., Calvo, J.P., Ordóñez, S., Jones, B.F. and **Cañaveras, J.C.** (2001) Petrographic and geochemical evidence for the formation of primary, bacterially induced lacustrine dolomite: La Roda 'white earth' (Pliocene, central Spain). *Sedimentology*, **48,** 897–915.

Gardner, R.A.M. and **Hendry, D.A.** (1995) Early silica diagenetic fabrics in Late Quaternary sediments, south India. *J. Geol. Soc.*, **152,** 183–192.

Goldsmith, J.R. and **Graf, D.L.** (1958) Relations between lattice constraints and composition of the Ca-Mg carbonates. *Am. Mineral.*, **43,** 84–101.

Goldsmith, J.R., Graf, D.L. and **Heard, H.C.** (1961) Lattice constants of the calcium-magnesium carbonates. *Am. Mineral.*, **46,** 453–457.

Hardy, R.G. and **Tucker, M.E.** (1988) X-ray powder diffraction of sediments. In: *Techniques in Sedimentology* (ed. M.E. Tucker), pp. 191–228. Blackwell Science Publs, Oxford.

Hesse, R. (1990) Silica diagenesis: origin of inorganic and replacement cherts. In: *Diagenesis, Geoscience Canada Reprint Series 4* (Eds I.A. McIlreath and D.W. Morrow), pp. 277–316. Geological Association of Canada, Canada.

Kinsman, D.J.J. (1964) The recent carbonate sediments near Halat al Bahrani, Trucial Coast. In: *Deltaic and Shallow Marine Deposits* (Ed. L.M.J.U. van Straaten), *Developments in Sedimentology*, **1,** 189–192.

Konhauser, K.O. (1998) Diversity of bacterial iron mineralization. *Earth-Sci. Rev.*, **43,** 91–121.

Konhauser, K.O., Fyfe, W.S., Ferris, F.G. and **Beveridge, T.J.** (1993) Metal sorption and mineral precipitation by bacteria in two Amazonian river systems: Rio Solimoes and Rio Negro, Brazil. *Geology*, **21,** 1103–1106.

Konhauser, K.O., Phoenix, V.R., Bottrell, S.H., Adams, D.G. and **Head, I.M.** (2001) Microbial–silica interactions in Icelandic hot spring sinter: possible analogues for some Precambrian siliceous stromatolites. *Sedimentology*, **48,** 415–433.

Last, W.M. (1990) Lacustrine dolomite – an overview of modern, Holocene, and Pleistocene occurrences. *Earth-Sci. Rev.*, **27,** 221–263.

Léveillé, R.J., Fyfe, W.S. and **Longstaffe, F.J.** (2000) Geomicrobiology of carbonate-silicate microbialites from Hawaian basaltic sea caves. *Chem. Geol.*, **169,** 339–355.

Machel, H.G. (2001) Bacterial and thermochemical sulphate reduction in diagenetic setting-old and new insights. *Sed. Geol.*, **140,** 143–175.

Mann, S., Douglas, D.A., Didymus, J.M., Douglas, T., Heywood, B.R., Meldrum, F.C. and **Reeves, N.J.** (1993) Crystallization at inorganic-organic interfaces: biominerals and biomimetic synthesis. *Science*, **261,** 1286–1292.

Mediavilla, R.M. and **Dabrio, C.J.** (1989) Las calizas del Páramo en el sur de la Provincia de Palencia. *Stvdia Geol. Salmanticensia*, **5,** 273–291.

Mediavilla, R., Dabrio, C., Martín Serrano, A. and **Santisteban, J.L.** (1996) Lacustrine Neogene systems of the Duero Basin: Evolution and controls. In: *Tertiary basins of Spain* (Eds P.F. Friend and C.J. Dabrio), pp. 228–236. Cambridge Univ. Press, Cambridge.

Moreira N.F., Walter, L.M., Vasconcelos, C., McKenzie, J.A. and **McCall, P.J.** (2004) Role of sulfide oxidation in dolomitization: sediment and pore-water geochemistry of a modern hypersaline lagoon system. *Geology*, **32,** 701–704.

Mukhopadhyay, J., Gutzmer, J. and **Beukes N.J.** (2004) Organotemplate silica deposition in Neoproterozoic deep-marine environments: evidence from the Penganga Group, Adilabad, India. *Terra Nova*, **16,** 338–343.

Noffke, N., Verdes, G. and **Klenke, T.** (2003) Benthic cyanobacteria and their influence on the sedimentary dynamics of peritidal depositional systems (siliciclastic, evaporitic salty, and evaporitic carbonatic). *Earth-Sci. Rev.*, **1279,** 1–14.

Ordóñez, S., López Aguayo, F. and **García del Cura, M.A.** (1981) Chemical carbonated sediments in continental basins: The Duero Basin. *Abstracts Book IAS. 2nd Eur Regional Meeting Bologna, Italy*, pp. 130–133.

Rao, V.P., Kessarkar, P.M., Krumbein, K.E., Krajewski, K.P. and **Schneider, R.J.** (2003) Microbial dolomite crust from the carbonate platform of Western India. *Sedimentology*, **50,** 819–830.

Reid, R.P, Visscher, P.T., Decho, A.W., Stolz, J.F., Bebout, B.M., Dupraz, C., Macintyre, I.G., Paerl, H.W., Pinckney, J.L., Prufert-Bebout, L., Steppe, T.F. and **DesMarais, D.J.** (2000) The role of microbes in accretion, lamination and early lithification of modern marine stromatolites. *Nature*, **406,** 989–992.

Reid, R.P., James, N.P., Macintyre, I.G., Dupraz, C.P. and **Burne, R.V.** (2003) Shark Bay stromatolites: microfabrics and reinterpretation of origins. *Facies*, **49,** 299–324.

Renaut, R.W., Jones, B. and **Tiercelin, J.J.** (1998) Rapid *in situ* silicification of microbes at Loburu hot springs, Lake Bogoria, Kenya rift Valley. *Sedimentology*, **45,** 1083–1103.

Rodríguez-Aranda, J.P. and **Calvo, J.P.** (1998) Trace fossils and rhizoliths as a tool for sedimentological and palaeoenvironmental analysis of ancient continental evaporite successions. *Palaeogeogr. Palaeoclimatol. Palaeoecol.*, **140,** 383–399.

Sánchez-Navas, A., Martín-Algarra, A. and **Nieto, F.** (1998) Bacterially-mediated authigenesis of clays in phosphate stromatolites. *Sedimentology*, **45,** 519–533.

Sanz-Montero, M.E., Rodríguez-Aranda, J.P. and **García del Cura, M.A.** (2005) Texturas diagenéticas de calcita desarrolladas sobre facies dolomíticas microbianas en el Mioceno de la Cuenca del Duero (zona de Cuéllar). *Macla*, **3,** 193–195.

Sanz-Montero, M.E., García del Cura, M.A. and **Rodríguez-Aranda, J.P.** (2006a) Facies dolomíticas de sistemas lacustres miocenos en las cuencas del Duero y de Madrid. Rasgos indicativos de su origen microbiano. *Geotemas*, **9,** 215–218.

Sanz-Montero, M.E, García del Cura, M.A. and **Rodríguez-Aranda, J.P.** (2006b) Mediación microbiana en la formación de barita en sistemas lacustres miocenos de las Cuencas del Duero y Madrid. *Macla*, **6,** 449–451.

Sanz-Montero, M.E., Rodríguez-Aranda, J.P. and **Calvo, J.P.** (2006c). Mediation of endoevaporitic microbial communities in early replacement of gypsum by dolomite. A case study from Miocene lake deposits of the Madrid Basin, Spain. *J. Sed. Res.*, **76,** 1257–1266.

Schultze-Lam, S. and **Beveridge, T.J.** (1994) Nucleation of celestite and strontianite on a cyanobacterial S-layer. *Appl. Environ. Microbiol.*, **60,** 447–453.

Schultze-Lam, S., Harauz, G. and **Beveridge, T.J.** (1992) Participation of a cyanobacterial S-layer in fine-grain mineral formation. *J. Bacteriol.*, **174,** 7971–7981.

Souza-Egipsy, V., Wierzchos, J., Ascaso, C. and **Nealson, K.H.** (2005) Mg-silica precipitation in fossilization mechanisms of sand tufa endolithic microbial community, Mono Lake (California). *Chem. Geol.*, **217,** 77–87.

Stal, L.J. (1995) Physiological ecology of cyanobacteria in microbial mats and other communities. *New Phytol.*, **131,** 1–32.

Tucker, M.E. and **Wright, V.P.** (1990) *Carbonate Sedimentology*. Blackwell scientific publications, Oxford, 482 pp.

Urrutia, M.M. and **Beveridge, T.J.** (1993) Mechanism of silicate binding to the bacterial cell wall in *Bacillus subtilis*. *J. Bacteriol.*, **175,** 1936–1945.

Van Lith, Y., Warthmann, R., Vasconcelos, C. and **McKenzie, J.A.** (2003) Microbial fossilization in carbonate sediments: a result of the bacterial surface involvement in dolomite precipitation. *Sedimentology*, **50,** 237–245.

Vasconcelos, C. and **McKenzie, J.A.** (1997) Microbial mediation of modern dolomite precipitation and diagenesis under anoxic conditions (Lagoa Vermelha, Rio de Janerio, Brazil). *J. Sed. Res.*, **67,** 378–390.

Vasconcelos, C., McKenzie, J.A., Bernasconi, S., Grujic, D. and **Tien, A.J.** (1995) Microbial mediation as a possible mechanism for natural dolomite formation at low temperatures. *Nature*, **377,** 220–222.

Vasconcelos, C., Warthmann, R., McKenzie, J.A., Visscher, P.T., Bittermann, A.G. and **van Lith, Y.** (2006) Lithifying microbial mats in Lagoa Vermelha, Brazil: Modern Precambrian relics? *Sed. Geol.*, **185,** 175–183.

Visscher, P.T. and **Stolz, J.F.** (2005) Microbial mats as bioreactors: populations, processes and products. *Paleogeogr. Paleoclimatol. Paleooecol.*, **219,** 87–100.

Visscher, P.T., Reid, R.P. and **Bebout, B.M.** (2000) Microscale observations of sulfate reduction: correlation of microbial activity with lithified micritic laminae in modern marine stromatolites. *Geology*, **28,** 919–922.

Warthmann, R., van Lith, Y., Vasconcelos, C., McKenzie, J.A. and **Karpoff, A.M.** (2000) Bacterially induced dolomite precipitation in anoxic culture experiments. *Geology*, **28,** 1091–1094.

Warthmann, R., Vasconcelos, C. and **McKenzie, J.A.** (2005) Lithifying microbial mats in Lagoa Vermelha, Brazil: A model system for Precambrian carbonate formation? *Geophys. Res. Abstr.*, **7,** 01630.

Watson, A. (1985) Structure, chemistry and origins of gypsum crusts in southern Tunisia and the Central Namib Desert. *Sedimentology*, **32,** 855–875.

Westall, F., Boni, L. and **Guerzoni, M.E.** (1995) The silicification of microorganisms. *Palaeontology*, **38,** 495–528.

Westall, F., Steele, A., Toporski, J., Walsh, M., Allen C., Guidry, S., Gibson, E. and **Chafetz, H.** (2000) Polymeric substances and biofilms as biomarkers in terrestrial materials: implications for extraterrestrial samples. *J. Geophys. Res. Planets*, **105,** 24,511–24,527.

Wopfner, H. (1978) Silcretes of northern South Australia and adjacent regions. In: *Silcrete in Australia* (ed. T. Langford-Smith), pp. 93–141. Department of Geography, University of New England Press, Armidale.

Wright, D.T. (1999) The role of sulphate-reducing bacteria and cyanobacteria in dolomite formation in distal ephemeral lakes of Coorong region, South Australia. *Sed. Geol.*, **126,** 147–157.

Wright, D.T. and **Wacey, D.** (2005) Precipitation of dolomite using sulphate-reducing bacteria from the Coorong Region, South Australia: significance and applications. *Sedimentology*, **52,** 987–1008.

Manuscript received 13 September 2006; revision accepted 19 September 2007